Redox Biology 49 (2022) 102217

Contents lists available at ScienceDirect

Redox Biology

journal homepage: www.elsevier.com/locate/redox

A detrimental role of NLRP6 in host iron metabolism during *Salmonella* infection

Qifeng Deng [a,1], Sidi Yang [b,1], Lanqing Sun [a], Kai Huang [c], Kedi Dong [a], Yuan Zhu [a], Yu Cao [a], Yuanyuan Li [a], Shuyan Wu [a,*], Rui Huang [a,**]

[a] Department of Medical Microbiology, School of Biology & Basic Medical Sciences, Medical College of Soochow University, No. 199, Ren Ai Road, Suzhou, Jiangsu, 215123, PR China

[b] Centre for Infection and Immunity Studies (CIIS), School of Medicine, Shenzhen Campus of Sun Yat-sen University, Shenzhen, Guangdong, 518107, PR China

[c] Cambridge-Suda Genomic Resource Center, Jiangsu Key Laboratory of Neuropsychiatric Diseases, Medical College of Soochow University, Suzhou, Jiangsu, 215123, PR China

ARTICLE INFO

Keywords:
NLRP6
Nutritional immunity
Iron metabolism
Ferroportin
Salmonella Typhimurium

ABSTRACT

Maintaining host iron homeostasis is an essential component of nutritional immunity responsible for sequestrating iron from pathogens and controlling infection. Nucleotide-oligomerization domain-like receptors (NLRs) contribute to cytoplasmic sensing and antimicrobial response orchestration. However, it remains unknown whether and how NLRs may regulate host iron metabolism, an important component of nutritional immunity. Here, we demonstrated that NLRP6, a member of the NLR family, has an unconventional role in regulating host iron metabolism that perturbs host resistance to bacterial infection. NLRP6 deficiency is advantageous for maintaining cellular iron homeostasis in both macrophages and enterocytes through increasing the unique iron exporter ferroportin-mediated iron efflux in a nuclear factor erythroid-derived 2–related factor 2 (NRF2)-dependent manner. Additional studies uncovered a novel mechanism underlying NRF2 regulation and operating through NLRP6/AKT interaction and that causes a decrease in AKT phosphorylation, which in turn reduces NRF2 nuclear translocation. In the absence of NLRP6, increased AKT activation promotes NRF2/KEAP1 dissociation *via* increasing mTOR-mediated p62 phosphorylation and downregulates KEAP1 transcription by promoting FOXO3A phosphorylation. Together, our observations provide new insights into the mechanism of nutritional immunity by revealing a novel function of NLRP6 in regulating iron metabolism, and suggest NLRP6 as a therapeutic target for limiting bacterial iron acquisition.

1. Introduction

Nutritional immunity, based on the restriction of essential transition metals' availability, is a key defense strategy against pathogenic microbes [1]. Iron, the most abundant transition metal in human, is a necessary nutrition element required for both humans and nearly all bacterial species, including *Salmonella enterica* serovar Typhimurium (*S.* Typhimurium) [2]. As a typical facultative intracellular bacterium, *S.* Typhimurium survives within macrophages, scavenging iron from its host to satisfy its nutrient requirements for growth and proliferation [3]. Therefore, regulating host iron metabolism and sequestrating iron away from invading pathogens is considered a potential therapeutic strategy against infectious diseases.

Host iron homeostasis is exquisitely governed by two regulatory systems. The first, termed systemic iron metabolism, relies primarily on hepcidin, a hormone mainly produced by hepatocytes. The second, known as cellular iron metabolism, coordinates the regulation of cellular iron import, storage, and export [4]. It is well established that these two homeostatic pathways intersect in the liver, where many of the iron-handling functions are modulated by liver macrophages [5]. Macrophages take up transferrin-bound iron *via* their transferrin receptor (TFR), capture non-transferrin-bound iron through another importer—the divalent metal transporter 1 (DMT1)—and preserve iron storage in ferritin. Of note, ferroportin (FPN) is the unique protein acting as iron exporter in mammals. FPN expression is regulated at the

* Corresponding author.
** Corresponding author.
E-mail addresses: wushuyan@suda.edu.cn (S. Wu), hruisdm@163.com (R. Huang).
[1] These authors contributed equally.

https://doi.org/10.1016/j.redox.2021.102217
Received 11 October 2021; Received in revised form 17 December 2021; Accepted 17 December 2021
Available online 18 December 2021

List of abbreviation

4EBP1	4E binding protein 1
ARNT	aryl hydrocarbon receptor nuclear translocator
BMDMs	bone marrow-derived macrophages
CFUs	colony-forming units
DAMPs	damage-associated molecular patterns
DFP	deferiprone
DMT1	divalent metal transporter 1
FPN	ferroportin
FBS	fetal bovine serum
FOXO3A	Forkhead box O3A
FTH	heavy chain of ferritin
HMOX1	heme oxygenase 1
HIF	hypoxia-inducible factor
IRE/IRP	iron response element/iron regulatory protein
KEAP1	Kelch-like ECH-associated protein 1
FTL	light chain of ferritin
LC3	microtubule-associated protein 1 light chain 3
MEFs	mouse embryonic fibroblasts
mTORC1	mammalian target of rapamycin complex 1
MLN	mesenteric lymph node
MTF1	metal regulatory transcription factor 1
MOI	multiplicity of infection
NQO1	NADPH quinone oxidoreductase 1
NDP52	nuclear domain 10 protein 52
NRF2	nuclear factor erythroid-derived 2–related factor 2
NLRs	Nucleotide-oligomerization domain-like receptors
p62/SQSTM1	p62/sequestosome 1
PAMPs	pathogen-associated molecular patterns
PRRs	pattern recognition receptors
S. Typhimurium	*Salmonella enterica* serovar Typhimurium
shRNA	short hairpin RNA
siRNA	small interfering RNA
TFR	transferrin receptor
TU	transducing unit

transcriptional level by several transcription factors, at the translational level by the iron response element/iron regulatory protein (IRE/IRP) system, and at the protein level, by hepcidin-induced FPN internalization and proteolysis [6]. Enhanced expression of FPN, which increases iron export and decreases intracellular iron accumulation in macrophages, is considered a protective antimicrobial response in host resistance to *S.* Typhimurium infection [7].

The innate immune system senses pathogen-associated molecular patterns (PAMPs) and damage-associated molecular patterns (DAMPs) through pattern recognition receptors (PRRs). The nucleotide-oligomerization domain-like receptors (NLRs) form a family of cytoplasmic PRRs that modulate inflammatory cytokines production and mediate regulated cell death (RCD). A growing body of evidence indicates that NLRs may be involved in the maintenance of metabolic homeostasis [8]. However, the link between NLRs and host iron metabolism, especially during bacterial infections, remains unclear.

In the present study, using well-established models of orally infected mouse *in vivo* and macrophage infection *in vitro*, we explore potential interconnections between the efficacy of the NLR-associated antimicrobial response, regulation of iron metabolism, and pathogenicity of *S.* Typhimurium. To the best of our knowledge, we provide the first evidence that NLRs participate in the regulation of iron homeostasis. NLRP6, a recently identified member of the NLR family, exerts a strong priming influence on host iron metabolism, leading to an intracellular iron overload that promotes *S.* Typhimurium growth and virulence. Our results identify a novel function for NLRP6 in modulating nutritional immunity and suggest NLRP6 as a therapeutic target for limiting bacterial iron acquisition.

2. Results

2.1. NLRP6 increases host susceptibility to S. Typhimurium infection and promotes the dysregulation of iron homeostasis

To investigate the contribution of NLRP6 to host defense and iron homeostasis, we first infected orally *Nlrp6*$^{-/-}$ mice and littermate wild-type control mice with *S.* Typhimurium. The infected *Nlrp6*$^{-/-}$ mice exhibited improved survival and lost significantly less body weight compared with similarly treated wild-type mice (Fig. 1, A and B). We further examine whether NLRP6 impacted the replication and survival of *S.* Typhimurium *in vivo*. Previous works from our laboratory and another showed that *S.* Typhimurium disseminates to systemic organs at three days post-infection [9,10]. As expected, the infected *Nlrp6*$^{-/-}$ mice had a much lower bacterial burden in colon, mesenteric lymph node (MLN), liver, and spleen, but not in the duodenum, relative to that of the wild-type controls at three days post-infection (Fig. 1C and Fig. S1A). The histopathological analysis revealed extensive morphologic changes in the colon, liver and spleen of the wild-type mice, compared with those of the *Nlrp6*$^{-/-}$ mice, characterizing by increased epithelial disruption and significant crypt loss in the colon (Fig. S1B); marked infiltration of inflammatory cells with substantial cell death in the liver (Fig. 1D and Fig. S1C); multifocal necrotizing splenitis and disruption of normal structure of the red and white pulp of the spleen (Fig. 1D and Fig. S1D). Moreover, no significant difference was observed between the duodenum of these two genotypes (Fig. S1E). Considering that dysregulation of host iron homeostasis, characterizing by hypoferremia and iron accumulation in systemic organs, is relevant to severe salmonellosis, we then asked whether NLRP6 could influence host iron metabolism *in vivo*. Serum iron concentration was markedly declined in orally infected wild-type mice, as previously reported [10]. However, *Nlrp6*$^{-/-}$ mice were resistant to the reduction in serum iron level, manifesting as a much higher serum iron content than the wild-type at three days post-infection (Fig. 1E). Accompanied by the changes of serum iron, Perls' staining on spleen sections revealed a higher accumulation of iron in wild-type than in *Nlrp6*$^{-/-}$ infected mice (Fig. 1F). Of note, the infected *Nlrp6*$^{-/-}$ mice exhibited a significantly lower level of non-heme iron in liver and spleen, compared with infected wild-type mice, while the effect of the knockout was modest on heme level (Fig. 1, G and H). In contrast, NLRP6 deficiency had no effect on non-heme or heme levels in the duodenum and the colon during infection (fig. S1, F and G). To characterize the cell types responsible for NLRP6-mediated changes in iron metabolism during infection, we measured non-heme and heme iron contents in non-parenchymal liver cells and hepatocytes isolated from wild-type and *Nlrp6*$^{-/-}$ mice. While no apparent differences in iron level were detected between wild-type and *Nlrp6*$^{-/-}$ hepatocytes, non-heme iron content, but not the level of heme, was markedly reduced in *Nlrp6*$^{-/-}$ non-parenchymal liver cells compared with their wild-type counterparts (Fig. 1, I and J). Taken together, these results suggest that NLRP6 is detrimental to the host control of *S.* Typhimurium infection and the maintenance of iron homeostasis.

2.2. NLRP6 regulates macrophage iron metabolism through FPN

Macrophages are main contributors to host protection against *S.* Typhimurium infection and regulate iron recycling [11,12]. Therefore, we sought to assess the potential impact of NLRP6 on iron metabolism in *S.* Typhimurium-infected macrophages. Non-heme iron level was significantly lower in macrophages isolated from *Nlrp6*$^{-/-}$ livers than in those from wild-type livers (Fig. 2A). To further decipher the role of NLRP6 in macrophage iron metabolism and whether these changes

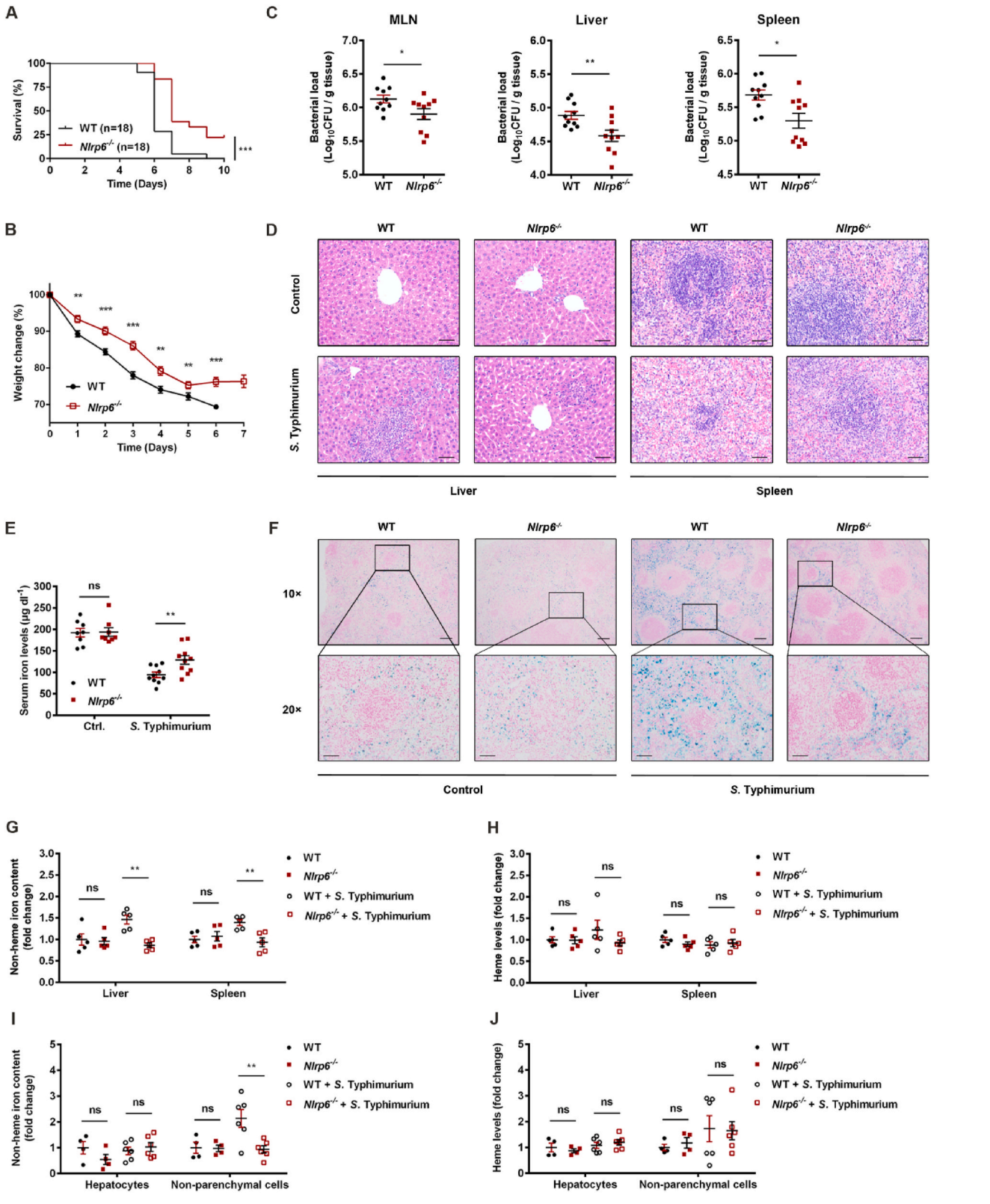

(caption on next page)

Fig. 1. *Nlrp6*-deficiency attenuates the dysregulation of iron metabolism and protects mice against infection with *S.* Typhimurium. Streptomycin-pretreated wild-type and *Nlrp6*$^{-/-}$ mice were orally infected with 1×10^7 CFUs of *S.* Typhimurium strain SL1344. (A) Survival in wild-type and *Nlrp6*$^{-/-}$ mice (n = 18 per group). Results were presented relative to initial values, set as 100% (throughout). (B) Percentage change in body weight during *S.* Typhimurium infection (n = 18 per group). Because of increased mortality in wild-type mice, weight assessments were halted on day 7. (C–J) Streptomycin-pretreated wild-type and *Nlrp6*$^{-/-}$ mice were orally infected with 1×10^7 CFUs of *S.* Typhimurium strain SL1344 and analyzed at 3 days post-infection. (C) Viable count of *S.* Typhimurium in MLN, liver and spleen (n = 10 per group). (D) Hematoxylin and eosin staining of liver and spleen sections. Original magnification, × 20; scale bars: 50 μm. Representative histopathological images are shown. (E) Serum iron levels (Ctrl., n = 8 per group; *S.* Typhimurium, n = 10 per group). (F) Perls' Prussian Blue staining of the spleen. scale bars: 50 μm. One of 3 representative histology experiments is shown. (G) Non-heme iron content in liver and spleen (n = 5 per group). (H) Heme levels in liver and spleen (n = 5 per group). (I) Non-heme iron content in primary hepatocytes and liver non-parenchymal cells (Ctrl., n = 4 per group; *S.* Typhimurium, n = 6 per group). (J) Heme levels in primary hepatocytes and liver non-parenchymal cells (Ctrl., n = 4 per group; *S.* Typhimurium, n = 6 per group). Data were compared with independent Student's *t*-test. Survival rates were estimated by the Gehan-Breslow-Wilcoxon test. Values are expressed as the mean ± SEM, and statistically significant differences are indicated. $^*P < 0.05$; $^{**}P < 0.01$; $^{***}P < 0.001$; ns, not significant. (For interpretation of the references to colour in this figure legend, the reader is referred to the Web version of this article.)

could occur at early infection stage as previously described [13], bone marrow-derived macrophages (BMDMs) were co-cultured with *S.* Typhimurium to establish an *in vitro* model of infection and analyzed at 4 h post-infection. Although NLRP6 deficiency did not affect phagocytosis of bacteria by the macrophages (Fig. S2A), at 4 h post-infection the *Nlrp6*$^{-/-}$ BMDMs had lower bacterial burden and non-heme content than the wild-type BMDMs (Fig. 2, B and C). Treatment with the iron chelator deferiprone (DFP) reduced *S.* Typhimurium intracellular proliferation and abolished the difference in bacterial loads between the wild-type and *Nlrp6*$^{-/-}$ BMDMs (Fig. 2B). To gain a better understanding of the mechanisms whereby NLRP6 modulates cellular iron metabolism, the expression of molecules involved in iron import, storage, and export was analyzed. At 4 h post-infection, the expression of the major iron acquisition regulatory genes *Tfr* and *Dmt1* was comparable in *Nlrp6*$^{-/-}$ and wild-type BMDMs (Fig. 2D). The expression of the major iron storage protein ferritin, composed of light chains encoded by the *Ftl* gene and heavy chains encoded by the *Fth1* gene, was higher in *Nlrp6*$^{-/-}$ than in wild-type BMDMs after infection. However, Western blot analysis did not detect any remarkable difference in either FTL or FTH protein levels between infected BMDMs with different genotypes (Fig. 2, E and F), suggesting that changes in expression of ferritin were not the major driver of NLRP6-mediated iron metabolic dysregulation. Importantly, in the presence of *S.* Typhimurium, the *Nlrp6*$^{-/-}$ BMDMs had significantly higher expression of the unique iron exporter FPN than the wild-type BMDMs, at both the mRNA and the protein levels (Fig. 2, G and H). Consistent with the above observation, iron export was notably higher in *Nlrp6*$^{-/-}$ than in wild-type infected BMDMs (Fig. 2I). Knockdown of *Fpn* in BMDMs using a small interfering RNA (siRNA) reversed the effect of NLRP6-deficiency on intracellular bacterial load and iron content (Fig. 2, J to L). As a complementary approach to confirm these findings, we also conducted studies in which NLRP6 was overexpressed in human THP-1 monocytic cells. Expectedly, the overexpression of NLRP6 enhanced intracellular bacterial load which could be reversed by DFP chelation, and decreased both the mRNA and protein levels of FPN in infected cells (fig. S2, B to E). These observations indicate that NLRP6 inhibits FPN expression, resulting in increased intracellular iron accumulation and bacterial burden.

2.3. NLRP6 regulates FPN transcription through NRF2

The expression of FPN is tightly regulated at the transcriptional, translational, and protein levels. Because our data showed that the levels of both FPN mRNA and protein were regulated by NLRP6, we hypothesized that this regulation occurred at the transcriptional level. As expected, treatment with the transcriptional inhibitor actinomycin D markedly reduced FPN mRNA levels in both wild-type and *Nlrp6*$^{-/-}$ infected BMDMs and reversed the effect of NLRP6-deficiency on FPN expression (Fig. 3A). Previous studies have reported that FPN transcription was modulated by three transcription factors, namely hypoxia-inducible factor (HIF), metal regulatory transcription factor 1 (MTF1), and nuclear factor erythroid-derived 2-related factor 2 (NRF2) [14–16]. To determine whether one of these pathways was relevant to FPN transcriptional regulation by NLRP6, *S.* Typhimurium-infected BMDMs and mouse embryonic fibroblasts (MEFs) were transfected with three pairs of siRNAs targeting aryl hydrocarbon receptor nuclear translocator (ARNT, encoding the obligatory dimer for HIF1-α and HIF2-α), MTF1, or NRF2 (Fig. 3B), and FPN mRNA level was monitored. Knockdown of either ARNT or MTF1 resulted in a reduction of FPN transcription, whereas FPN mRNA levels was still higher in *Nlrp6*$^{-/-}$ than in wild-type infected cells (Fig. 3, C and D), indicating that HIF and MTF1 were independent of this process. However, the increase of FPN mRNA caused by NLRP6 deficiency in infected cells was reversed by NRF2 knockdown (Fig. 3E). In line with this observation, suppression of NRF2 enhanced intracellular bacterial burden and iron content in infected BMDMs and eliminated the difference initially seen between the wild-type and *Nlrp6*$^{-/-}$ BMDMs (Fig. 3, F and G). These results suggest that NLRP6 regulates iron homeostasis and FPN transcription in a NRF2-dependent manner during infection. We further explored whether NLRP6 mediated NRF2 inhibition. At 4 h post-infection, *Nlrp6*$^{-/-}$ BMDMs expressed an amount of NRF2 protein significantly higher than the wild-type, whereas no significant difference in NRF2 mRNA level was detected between the BMDMs of these two genotypes (Fig. 3, H and I). At the same timepoint, the transcriptional level of two prototypical NRF2 target genes, namely NADPH quinone oxidoreductase 1 (NQO1) and heme oxygenase 1 (HMOX1), was significantly higher in *Nlrp6*$^{-/-}$ than in wild-type BMDMs (Fig. 3J). Consistently, overexpression of NLRP6 in infected cells decreased NRF2 nuclear translocation, reduced NRF2 protein level, and lowered NQO1 mRNA level (Figs. S2 and F and Fig. 3, K and L). These results demonstrate that NLRP6 decreases FPN transcription through precluding NRF2 activity.

2.4. NLRP6 is required for autophagy induction upon S. Typhimurium infection

Next, we focused our study on the mechanism whereby NLRP6 could regulate NRF2. Dysregulated autophagy has been previously shown to prolong NRF2 activation [17]. Therefore, we sought to determine whether NLRP6 impacted autophagy in response to *S.* Typhimurium infection. For this purpose, cells carrying a NLRP6-expressing plasmid or corresponding empty control vector were transfected with RFP-GFP-LC3, a widely used autophagic indicator with yellow LC3 signal representing autophagosome (with both GFP and RFP signals) and red LC3 signal when in the autolysosome due to the acidic milieu that quenches GFP signal [18], and subsequently infected with *S.* Typhimurium. Analysis by immunofluorescence 6 h after infection showed that the amount of both the yellow LC3 puncta and the red puncta were lower in control cells than in cells overexpressing NLRP6 (Fig. 4A). The conversion rate of the cytosol-located LC3-I form into the autophagosome-associated lapidated LC3-II form is widely used to assess autophagic activity. As shown in Fig. 4B, no significant difference in the protein level of total LC3 was observed between wild-type and *Nlrp6*$^{-/-}$ BMDMs. However, a progressive increase of the LC3-II/LC3-I ratio was found in *S.* Typhimurium-infected wild-type BMDMs, whereas no significant changes were observed in *Nlrp6*$^{-/-}$ BMDMs

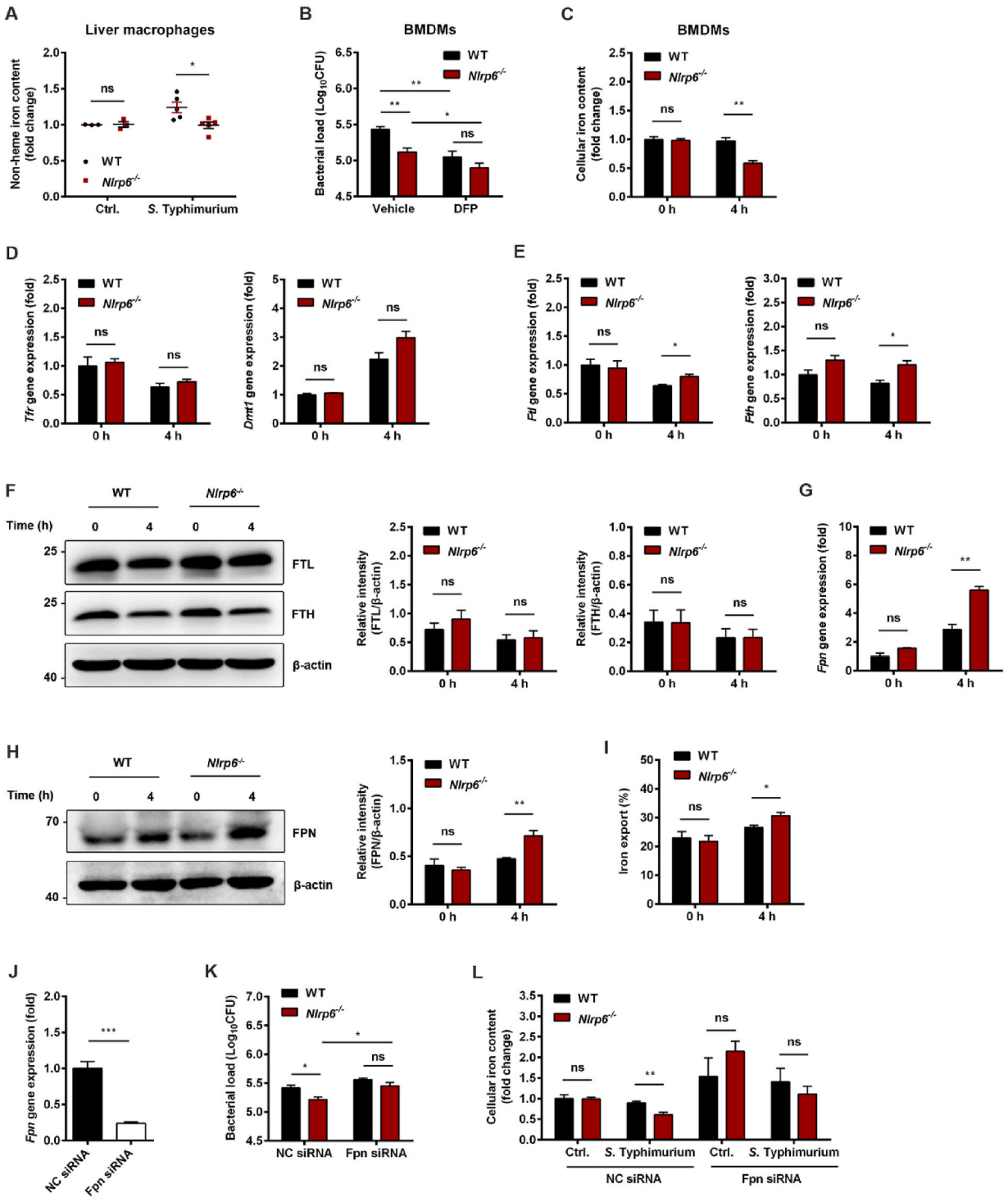

Fig. 2. Increased FPN expression in *Nlrp6*$^{-/-}$ macrophages favors the maintenance of iron homeostasis during *S.* Typhimurium infection. (A) Streptomycin-pretreated wild-type and *Nlrp6*$^{-/-}$ mice were orally infected with 1×10^7 CFUs of *S.* Typhimurium strain SL1344 and analyzed at 3 days post-infection. Non-heme iron content in isolated liver macrophages (Ctrl., n = 3 per group; *S.* Typhimurium, n = 5 per group). (B) BMDMs isolated from wild-type and *Nlrp6*$^{-/-}$ mice were treated with either vehicle or 50 μM DFP for 30 min and then infected with *S.* Typhimurium strain SL1344 at an MOI of 10. Viable count of intracellular *S.* Typhimurium at 4 h post-infection (n = 4 independent experiments). (C–I) BMDMs isolated from wild-type and *Nlrp6*$^{-/-}$ mice were infected with *S.* Typhimurium strain SL1344 at an MOI of 10 and analyzed at 4 h post-infection. (C) Non-heme iron content in BMDMs (n = 4 independent experiments). (D) Quantitative PCR analysis of *Tfr* and *Dmt1* (n = 4 independent experiments). (E) Quantitative PCR analysis of *Ftl* and *Fth* (n = 4 independent experiments). (F) Western blot analysis and relative intensity of FTL and FTH (n = 4 independent experiments). (G) Quantitative PCR analysis of *Fpn* (n = 4 independent experiments). (H) Western blot analysis and relative intensity of FPN (n = 4 independent experiments). (I) Iron export (n = 4 independent experiments). (J) BMDMs isolated from wild-type and *Nlrp6*$^{-/-}$ mice were transfected with either 50 nM negative-control siRNA or 50 nM siRNA specific for Fpn for 48 h. Quantitative PCR analysis of *Fpn* (n = 4 independent experiments). (K, L) BMDMs isolated from wild-type and *Nlrp6*$^{-/-}$ mice were transfected with either 50 nM negative-control siRNA or 50 nM siRNA specific for Fpn. After 48 h of incubation, BMDMs were infected with *S.* Typhimurium strain SL1344 at an MOI of 10 and analyzed at 4 h post-infection. (K) Viable count of intracellular *S.* Typhimurium (n = 4 independent experiments). (L) Non-heme iron content in BMDMs (n = 4 independent experiments). Data were compared with independent Student's *t*-test. Values are expressed as the mean ± SEM, and statistically significant differences are indicated. $^*P < 0.05$; $^{**}P < 0.01$; $^{***}P < 0.001$; ns, not significant.

(Fig. 4B). LC3-II reduction might result either from enhanced autophagosome clearance or, alternatively, from impaired induction of autophagy [19]. Hence, macrophages were treated with bafilomycin A1 (BafA1), a blocker of autophagosome/lysosome fusion. BafA1 treatment resulted in a remarkable increase of LC3-II. However, upon *S.* Typhimurium infection the LC3-II/LC3-I ratio was still lower in *Nlrp6*$^{-/-}$ than in wild-type BMDMs (Fig. S3A and Fig. 4C), confirming that this decrease was due to reduced autophagic flux. Furthermore, loss of NLRP6 had no significant effect on the transcriptional level of LC3 and lysosomal-associated membrane protein 1 (LAMP1), or on the expression of autophagy-related gene 5 (ATG5) and autophagy-related gene 16-like 1 (ATG16L1) (Fig. 4, D and E and fig. S3, B and C).

Recent studies have identified five autophagy receptors that participate in autophagy process, namely: NBR1 autophagy cargo receptor (NBR1), Tax1 binding protein 1 (TAX1BP1), optineurin (OPTN), p62/sequestosome 1 (p62/SQSTM1) and calcium binding and coiled-coil domain 2/nuclear domain 10 protein 52 (CALCOCO2/NDP52) [20]. We further investigated which autophagy receptor(s) were involved in NLRP6-mediated autophagy during *S.* Typhimurium infection. The mRNA levels of all five autophagy receptors in *Nlrp6*$^{-/-}$ and wild-type BMDMs were comparable (Fig. S3D). At four and 8 h post-infection, no significant difference in the protein levels of NBR1, TAX1BP1 and OPTN was observed between wild-type and *Nlrp6*$^{-/-}$ BMDMs. However, the protein level of p62 and NDP52 was dramatically higher in *Nlrp6*$^{-/-}$ than in wild-type BMDMs at 4 h post-infection (Fig. 4F). Moreover, the *Nlrp6*$^{-/-}$ BMDMs had significantly higher protein level of NDP52 than the wild-type BMDMs at 8 h post-infection. (Fig. 4F). These results suggest that NLRP6 increases autophagic flux and causes a decrease in p62 and NDP52 protein levels during *S.* Typhimurium infection.

2.5. The regulation of KEAP1/NRF2 signaling by NLRP6 is mediated through AKT-driven phosphorylation of p62 and FOXO3A

Phosphorylation of p62 at Ser351 by mammalian target of rapamycin complex 1 (mTORC1) was suggested to act as a bridge between autophagy and NRF2 signaling [21,22]. We wondered whether this autophagy receptor protein could be involved in the reduction of NRF2 caused by NLRP6. As predicted, *S.* Typhimurium infection led to an increase in phosphorylation of p62 and 4E binding protein 1 (4EBP1), a well-known substrate of mTORC1. Importantly, the phosphorylation levels of these two proteins were dramatically higher in *Nlrp6*$^{-/-}$ BMDMs compared with wild-type (Fig. 5, A and B). Treatment with the mTORC1 inhibitor Rapamycin (Rap) resulted in a significant reduction of p62 and 4EBP1 phosphorylation, and no significant difference in p62 phosphorylation was detected between wild-type and *Nlrp6*$^{-/-}$ BMDMs after downregulation of mTORC1 activity (Fig. 5C). These results, taken together with the data presented in Fig. 4, indicated conclusively that NLRP6 decreases the phosphorylation level of p62 by utilizing at least two mechanisms: i) by increasing autophagic activity which resulted in a decrease of the autophagy substrate p62. ii) by downregulating mTORC1-mediated phosphorylation mechanism. However, Nqo1 mRNA level was still higher in *Nlrp6*$^{-/-}$ than in wild-type infected BMDMs (Fig. 5D). We next investigated whether NLRP6 regulated the expression of Kelch-like ECH-associated protein 1 (KEAP1), a main negative modulator of NRF2 [23]. Quantitative PCR and Western blot analyses on cells taken 4 h after infection showed that loss of NLRP6 significantly decreased KEAP1 expression at both the mRNA and protein levels (Fig. 5, E and F). A luciferase reporter assay further showed that overexpression of NLRP6 increased *KEAP1* promoter activity (Fig. 5G). Since KEAP1 is transcriptionally regulated by the transcription factor Forkhead box O3A (FOXO3A) [24], we assessed whether FOXO3A was involved in NLRP6-mediated KEAP1 induction. Overexpression of NLRP6 in either HeLa or THP-1 cells significantly enhanced FOXO3A nuclear translocation upon *S.* Typhimurium infection (Fig. 5H and Fig. S4A). Moreover, 4 h post-infection, the level of FOXO3A phosphorylation was significantly higher in *Nlrp6*$^{-/-}$ than in wild-type BMDMs (Fig. 5I). These data suggest that NLRP6 may have an effect on key molecules acting upstream of mTORC1 and FOXO3A and inhibiting the phosphorylation of these two proteins.

Previous studies have demonstrated that the serine/threonine kinase AKT, a key regulator of cell survival and metabolism, can directly and indirectly phosphorylate many downstream enzymes and transcription factors [25]. Among them, mTORC1 was found to be indirectly phosphorylated by AKT through inhibition of tuberous sclerosis complex 2, while FOXO3A is directly phosphorylated by AKT, which induces its translocation into the cytoplasm [24,26]. Therefore, we further tested the possibility that NLRP6 could directly mediate the phosphorylation of AKT and subsequently regulate KEAP1/NRF2 pathway. Of note, *S.* Typhimurium infection induced a significant elevation of AKT phosphorylation at Ser473 in *Nlrp6*$^{-/-}$ BMDMs as compared to wild-type BMDMs (Fig. 5J). Immunoprecipitation assays showed physical interactions between NLRP6 and AKT (Fig. 5K and Fig. S4B). Although it has been reported that lysine-63 (K63) polyubiquitination is involved in phosphorylation of AKT at Ser473, no significant difference in K63-linked ubiquitination of AKT was observed between cells transfected with a NLRP6-expressing plasmid or the control vector (Fig. S4C). To verify if NLRP6-associated AKT suppression was involved in regulating macrophage iron metabolism, *S.* Typhimurium-infected BMDMs were treated with the AKT inhibitor MK2206. Notably, the addition of MK2206 led to an increase in intracellular non-heme iron content and could rescue the reduction of iron level in *Nlrp6*$^{-/-}$ BMDMs to a large degree (Fig. 5L). In parallel to this phenotype, differential mRNA levels of FPN, NQO1, and KEAP1, and differential phosphorylation levels of p62 and FOXO3A caused by NLRP6 deficiency were also abrogated by pharmacological inhibition of AKT (Fig. 5, M and N), suggesting that suppression of AKT activity caused by NLRP6 decreases NRF2-mediated FPN transcription, in turn, lead to an increase of intracellular iron accumulation. Collectively, these findings indicate that NLRP6 inhibits NRF2 activity by utilizing at least two mechanisms: i) by decreasing p62 phosphorylation through AKT-mediated mTORC1-kinase activity. ii) by increasing KEAP1 transcription through AKT-induced FOXO3A phosphorylation.

2.6. NLRP6 modulates enterocyte iron metabolism during S. Typhimurium infection

To investigate if NLRP6 was involved in the regulation of enterocyte iron homeostasis, wild-type and *NLRP6*$^{-/-}$ Caco-2 intestinal epithelial cells were used to establish an *in vitro* model of *S.* Typhimurium infection. NLRP6 deficiency had no significant effect on the adhesion and invasion of bacteria (Figs. S5A and B) and exhibited no significant effects on the bacterial load at 4 h post-infection (Fig. S5C). However, *NLRP6*$^{-/-}$ Caco-2 cells had a lower intracellular bacterial burden and non-heme content compared with wild-type Caco-2 cells at 16 h post-infection (Fig. S5C and Fig. 6A), suggesting that NLRP6-mediated dysregulation of enterocyte iron metabolism mainly occur at late stage of infection. Concomitantly, both the mRNA and protein levels of FPN were significantly higher in *S.* Typhimurium-infected *NLRP6*$^{-/-}$ Caco-2 cells than in wild-type Caco-2 cells (Fig. 6, B and C). Similar to our observation in primary macrophage cultures, elevated active AKT was observed in *S.* Typhimurium-infected *NLRP6*$^{-/-}$ Caco-2 cells, which subsequently facilitated NRF2 accumulation and activation (Fig. 6, D–F). Treatment of Caco-2 cells with MK2206 attenuated NLRP6-mediated intracellular accumulation of iron, suppression of NRF2 activity, and reduction of FPN transcription (Fig. 6, G and H). In addition, NLRP6 deficiency significantly reduced LC3-I to –II conversion and increased the accumulation of p62 and NDP52 after infection (Fig. 6, I and J). These observations demonstrate that NLRP6 influences iron metabolism in intestinal epithelial cells during *S.* Typhimurium infection.

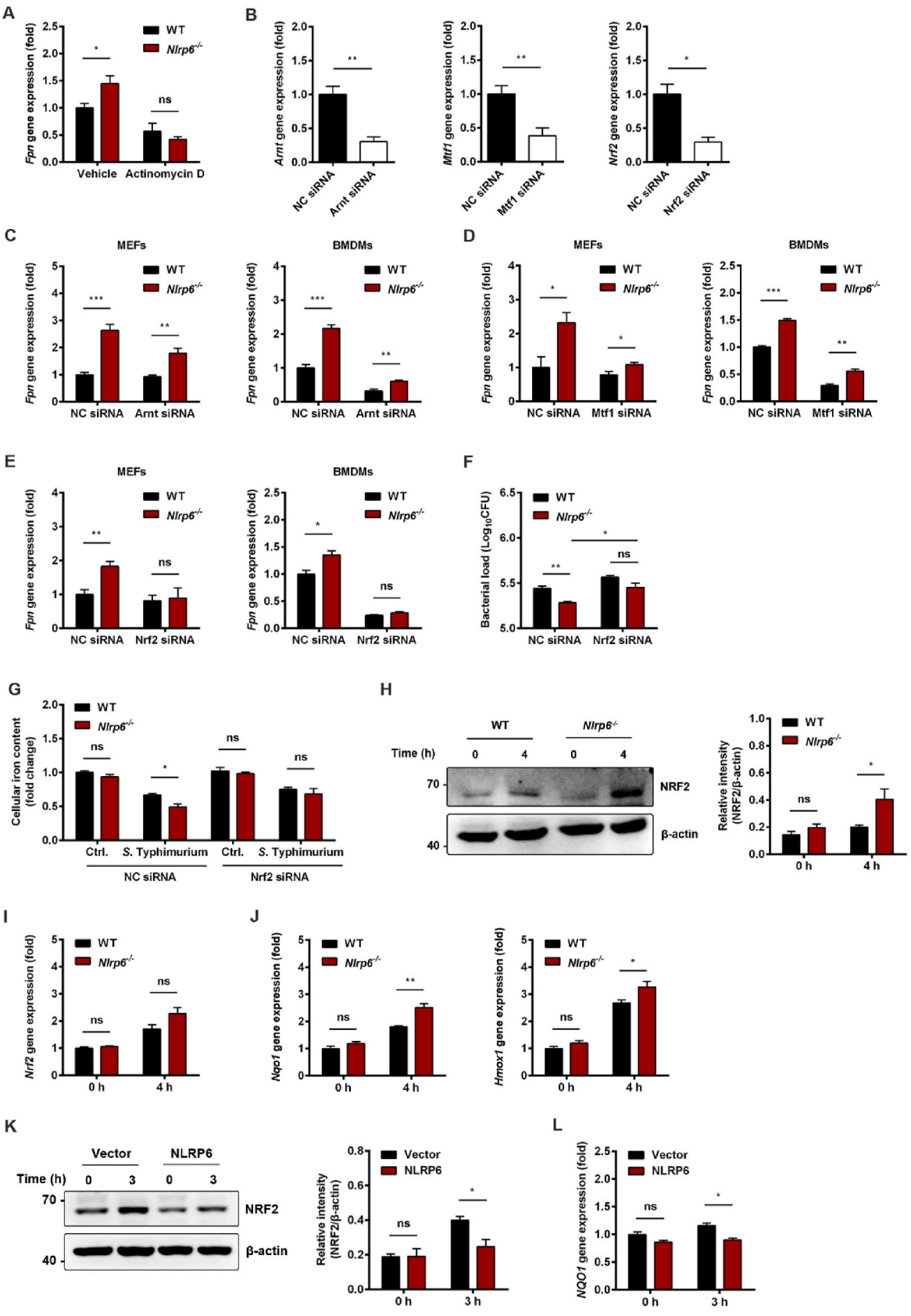

(caption on next page)

Fig. 3. NLRP6-mediated regulation of FPN transcription is dependent on NRF2. (A) BMDMs isolated from wild-type and *Nlrp6*$^{-/-}$ mice were treated with either vehicle or 5 μM actinomycin D. After 2 h of incubation, BMDMs were infected with *S.* Typhimurium strain SL1344 at an MOI of 10 and analyzed at 4 h post-infection. Quantitative PCR analysis of *Fpn* (n = 4 independent experiments). (B) MEFs isolated from wild-type and *Nlrp6*$^{-/-}$ mice were transfected with either 50 nM negative-control siRNA or 50 nM siRNA specific for Arnt, Mtf1 or Nrf2 for 48 h. Quantitative PCR analysis of *Arnt*, *Mtf1* and *Nrf2* (n = 3–5 independent experiments). (C) MEFs or BMDMs isolated from wild-type and *Nlrp6*$^{-/-}$ mice were transfected with either 50 nM negative-control siRNA or 50 nM siRNA specific for Arnt. After 48 h of incubation, cells were infected with *S.* Typhimurium strain SL1344 at an MOI of 10 and analyzed at 4 h post-infection. Quantitative PCR analysis of *Fpn* (n = 4 independent experiments). (D) MEFs or BMDMs isolated from wild-type and *Nlrp6*$^{-/-}$ mice were transfected with either 50 nM negative-control siRNA or 50 nM siRNA specific for Mtf1. After 48 h of incubation, cells were infected with *S.* Typhimurium strain SL1344 at an MOI of 10 and analyzed at 4 h post-infection. Quantitative PCR analysis of *Fpn* (n = 4 independent experiments). (E–G) MEFs or BMDMs isolated from wild-type and *Nlrp6*$^{-/-}$ mice were transfected with either 50 nM negative control siRNA or 50 nM siRNA specific for Nrf2. After 48 h of incubation, cells were infected with *S.* Typhimurium strain SL1344 at an MOI of 10 and analyzed at 4 h post-infection. (E) Quantitative PCR analysis of *Fpn* (n = 4 independent experiments). (F) Viable count of intracellular *S.* Typhimurium in BMDMs (n = 4 independent experiments). (G) Non-heme iron content in BMDMs (n = 4 independent experiments). (H–J) BMDMs isolated from wild-type and *Nlrp6*$^{-/-}$ mice were infected with *S.* Typhimurium strain SL1344 at an MOI of 10 and analyzed at 4 h post-infection. (H) Western blot analysis and relative intensity of NRF2 (n = 4 independent experiments). (I) Quantitative PCR analysis of *Nrf2* (n = 4 independent experiments). (J) Quantitative PCR analysis of *Nqo1* and *Hmox1* (n = 4 independent experiments). (K, L) THP-1 macrophages transfected with either an empty vector or His-NLRP6 were infected with *S.* Typhimurium strain SL1344 at an MOI of 10 and analyzed at 3 h post-infection. (K) Western blot analysis and relative intensity of NRF2 (n = 3 independent experiments). (L) Quantitative PCR analysis of *NQO1* (n = 3 independent experiments). Data were compared with independent Student's *t*-test. Values are expressed as the mean ± SEM, and statistically significant differences are indicated. $^{*}P < 0.05$; $^{**}P < 0.01$; $^{***}P < 0.001$; ns, not significant.

2.7. NLRP6-mediated NRF2 regulation of FPN contributes to S. Typhimurium-induced iron metabolic dysregulation in vivo

To understand better the observed effects of NLRP6 on macrophage and enterocyte iron homeostasis, NRF2 and FPN expression in duodenum, liver, and spleen were quantified by western blotting. Consistent with our *in vitro* observations, NRF2 and FPN protein levels were significantly higher in *S.* Typhimurium-infected *Nlrp6*$^{-/-}$ mice than in wild-type mice (Fig. 7, A and B and Fig. S6A). To test whether the inhibition of NRF2 could reverse this phenotype, *S.* Typhimurium-infected mice were intravenously injected with a lentivirus expressing a short hairpin RNA (shRNA) targeting Nrf2 mRNA or the control vector. NRF2 knockdown increased *S.* Typhimurium burden in both the liver and spleen, and eliminated the difference initially seen between wild-type and *Nlrp6*$^{-/-}$ mice (Fig. 7C). Nrf2 shRNA administration resulted in comparable levels of serum, hepatic and splenic iron in wild-type and *Nlrp6*$^{-/-}$ mice (Fig. 7, D and E). Moreover, downregulation of NRF2 reversed the reduction of non-heme iron content and the accumulation of FPN protein in liver macrophages caused by NLRP6 deficiency (Fig. 7, F and G). These findings indicated that NRF2 plays an important role in NLRP6-associated iron metabolic disorders occurring during *S.* Typhimurium infection *in vivo*.

2.8. NLRP6 regulates NRF2-mediated expression of FPN and host resistance to S. Typhimurium infection via modulating AKT activation in vivo

To further confirm the effects of AKT on NLRP6-mediated enhancement of bacteria load and iron metabolic dysregulation, *S.* Typhimurium-infected mice were orally administrated with the AKT inhibitor MK2206. The significant difference in tissue bacterial burden, serum iron, and tissue non-heme iron content between the wild-type and the *Nlrp6*$^{-/-}$ mice was abrogated by MK2206 (Fig. 8, A–C). Consistent with increased non-heme iron levels in liver macrophages, *Nlrp6*$^{-/-}$ mice treated with MK2206 had decreased level of FPN protein in these macrophages (Fig. 8, D and E). Suppression of AKT activity resulted in similar protein levels of NRF2 and KEAP1 in liver macrophages of the wild-type and the *Nlrp6*$^{-/-}$ mice, consistent with the absence of significant difference in AKT, 4EBP1, and FOXO3A phosphorylation between these mice (Fig. 8E). These *in vivo* data further support our results obtained *in vitro*, showing that NLRP6 regulates NRF2-mediated FPN expression and iron metabolism through AKT inhibition during *S.* Typhimurium infection.

3. Discussion

Iron occupies an essential position at the host-pathogen interface [27]. Here, we provide new insights into nutritional immunity by demonstrating that NLRP6, a member of the NLRs family, is associated with the dysregulation of host iron metabolism provoked by *S.* Typhimurium infection. We show that NLRP6 physically interacts with AKT, which leads to decreased AKT phosphorylation. The suppression of AKT activity decreases NRF2 nuclear translocation by both increasing NRF2/KEAP1 interaction *via* decreasing mTOR-mediated p62 phosphorylation, and upregulating KEAP1 transcription through the downregulation of FOXO3A phosphorylation. The decrease in NRF2 activation subsequently results in a reduction in its transcriptional target gene *Fpn*, thus ultimately decreasing FPN-mediated iron export, increasing intracellular iron content, and promoting *S.* Typhimurium survival (Fig. 8F). Our results provide new insights into the molecular mechanism of nutritional immunity by revealing that part of the effect of NLRP6 during intracellular pathogens infection results from the modulation of host iron metabolism.

NLRP6 has been shown to exert cell type- or tissue-specific functions in host defense against microbial infections. NLRP6 plays a protective role in *Citrobacter rodentium*-infected mice *via* regulating goblet cell mucus secretion [28]. In contrast, NLRP6 acts as a negative regulator of neutrophil innate immune response during infection with Gram-positive bacteria such as *Listeria monocytogenes* and *Staphylococcus aureus*, and NRLP6 deficiency is conducive to increased bacterial clearance and improved survival of infected mice [29]. As reported more recently by Hara et al., NLRP6 is able to directly bind and recognize the lipoteichoic acid produced by Gram-positive bacteria and subsequently initiate inflammation [30]. Using a mouse model of intraperitoneal infection with *S.* Typhimurium, one of the most common Gram-negative bacteria, Anand et al. demonstrated that NLRP6 worsens the course and outcome of infection [31]. However, *S.* Typhimurium infection is usually acquired orally [32]. Whether NLRP6 influences host defense in mice infected with *S.* Typhimurium *via* the natural route had remained poorly understood. Thus, for the current study, we established a streptomycin-pretreated mouse model of oral infection. Our data demonstrated that NLRP6 deficiency promotes host resistance against *S.* Typhimurium infection, as illustrated by the significantly lower mortality, body weight loss, bacterial load, and inflammatory tissue injury found in the *Nlrp6*$^{-/-}$ mice compared with wild-type. Previous study reported that the number of *S.* Typhimurium in duodenum reached a peak at 24–36 h post oral infection and subsequent decreased after 2 days post inoculation [33]. Our results supported these previous observations showing that the infected *Nlrp6*$^{-/-}$ mice had a much lower bacterial burden in the duodenum than those of the wild-type mice at 18 h post-infection (data not shown), whereas NLRP6 deficiency had no significant effects on duodenal bacterial loads and histological changes at three days post-infection (Figs. S1A and E), and no S. Typhimurium was detected in the duodenum at 5 days post infection (data not shown).

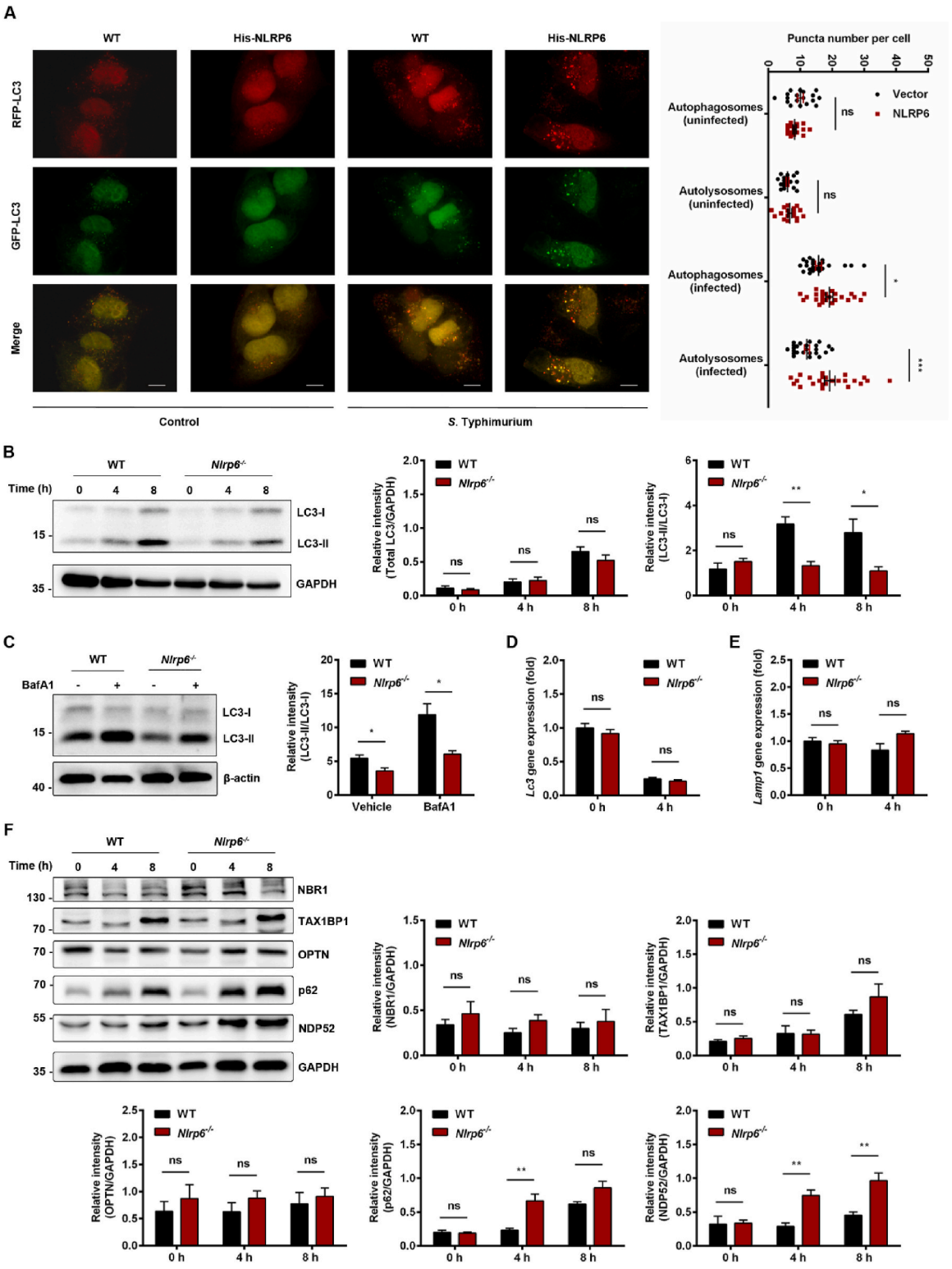

Fig. 4. Loss of *Nlrp6* impairs autophagy during *S.* Typhimurium infection. (A) HeLa cells were transfected with GFP-RFP-LC3 together with either an empty vector or His-NLRP6. After 36 h of incubation, HeLa cells were infected with *S.* Typhimurium strain SL1344 at an MOI of 10 and analyzed at 6 h post-infection. Fluorescence microscopic analysis of LC3. (Uninfected, 18 cells per group; Infected, 24 cells per group; n = 3 independent experiments). Original magnification, × 100; scale bars, 10 μm. Representative fluorescence images are shown. The number of LC3 puncta was counted using ImageJ Launcher broken symmetry software program. (B, D–F) BMDMs isolated from wild-type and *Nlrp6*$^{-/-}$ mice were infected with *S.* Typhimurium strain SL1344 at an MOI of 10 for the indicated time points. (B) Western blot analysis and relative intensity of LC3 (n = 4 independent experiments). (C) BMDMs isolated from wild-type and *Nlrp6*$^{-/-}$ mice were treated with either vehicle or 200 nM BafA1 for 4 h and then infected with *S.* Typhimurium strain SL1344 at an MOI of 10. Western blot analysis and relative intensity of LC3 at 4 h post-infection (n = 4 independent experiments). (D) Quantitative PCR analysis of *Lc3* (n = 4 independent experiments). (E) Quantitative PCR analysis of *Lamp1* (n = 4 independent experiments). (F) Western blot analysis and relative intensity of NBR1, TAX1BP1, OPTN, p62 and NDP52 (n = 4 independent experiments). Data were compared with independent Student's *t*-test. Values are expressed as the mean ± SEM, and statistically significant differences are indicated. *$P < 0.05$; **$P < 0.01$; ***$P < 0.001$; ns, not significant.

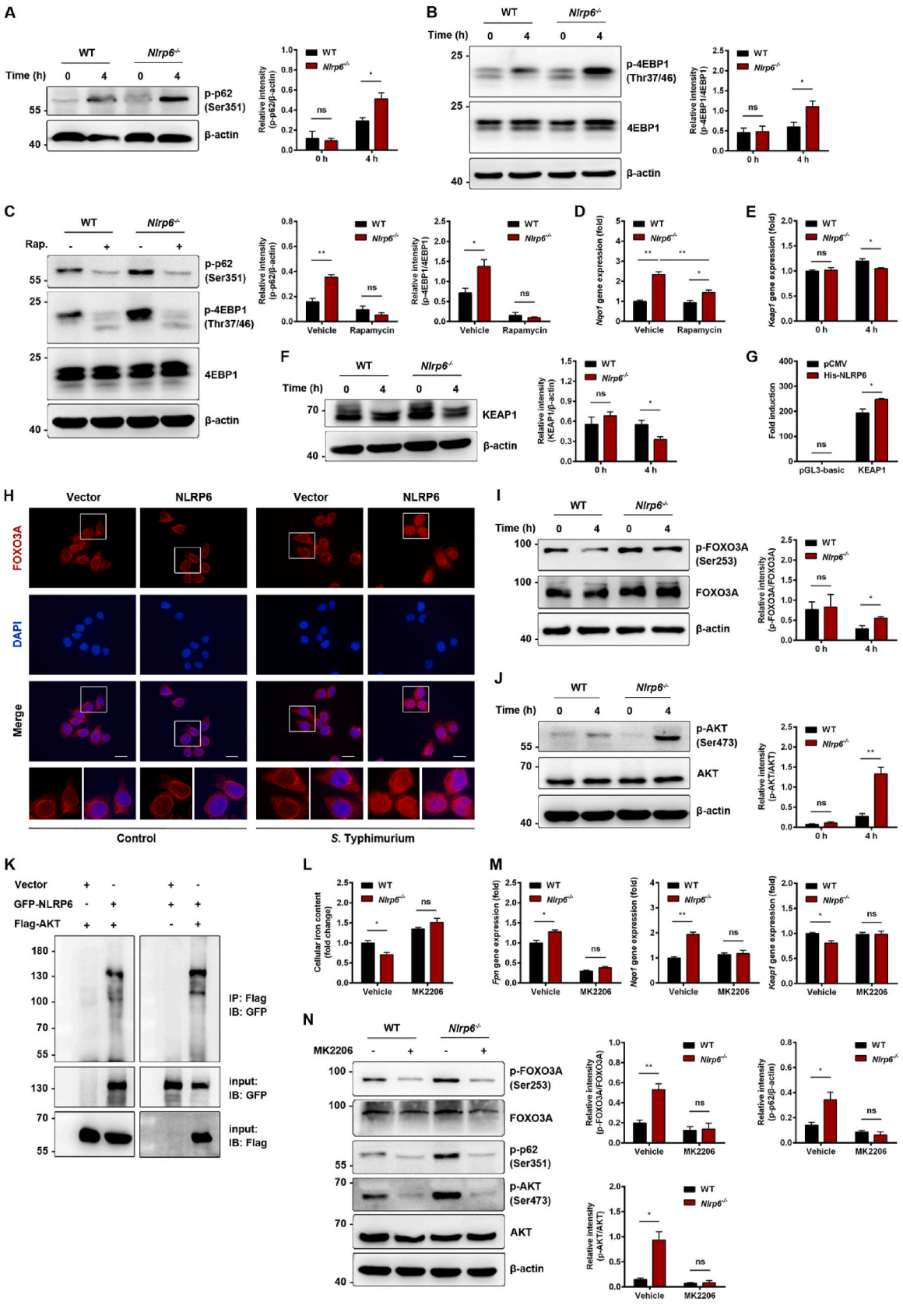

(caption on next page)

Fig. 5. NLRP6 interacts with AKT and regulates NRF2 activation *via* AKT-mediated phosphorylation of p62 and FOXO3A. (A, B) BMDMs isolated from wild-type and *Nlrp6*$^{-/-}$ mice were infected with *S*. Typhimurium strain SL1344 at an MOI of 10 and analyzed at 4 h post-infection. (A) Western blot analysis and relative intensity of p-p62 (Ser351) (n = 4 independent experiments). (B) Western blot analysis and relative intensity of p-4EBP1 (Thr37/46) and 4EBP1 (n = 4 independent experiments). (C, D) BMDMs isolated from wild-type and *Nlrp6*$^{-/-}$ mice were treated with either vehicle or 1 μM Rapamycin for 6 h and then infected with *S*. Typhimurium strain SL1344 at an MOI of 10 for 4 h. (C) Western blot analysis and relative intensity of p-4EBP1 (Thr37/46), 4EBP1 and p-p62 (Ser351) (n = 4 independent experiments). (D) Quantitative PCR analysis of *Nqo1* (n = 4 independent experiments). (E, F) BMDMs isolated from wild-type and *Nlrp6*$^{-/-}$ mice were infected with *S*. Typhimurium strain SL1344 at an MOI of 10 and analyzed at 4 h post-infection. (E) Quantitative PCR analysis of *Keap1* (n = 4 independent experiments). (F) Western blot analysis and relative intensity of KEAP1 (n = 4 independent experiments). (G) HEK293T cells were transfected with KEAP1 luciferase reporter plasmid together with either an empty vector or His-NLRP6. A plasmid expressing Renilla luciferase was co-transfected as an internal control. KEAP1 luciferase activity at 24 h post-transfection (n = 5 independent experiments). (H) HeLa cells transfected with either an empty vector or His-NLRP6 were infected with *S*. Typhimurium strain SL1344 at an MOI of 10 and analyzed at 6 h post-infection. Immunofluorescence microscopic analysis of the subcellular distribution of FOXO3A. Original magnification, × 40; scale bars, 50 μm. Representative fluorescence images are shown. (I, J) BMDMs isolated from wild-type and *Nlrp6*$^{-/-}$ mice were infected with *S*. Typhimurium strain SL1344 at an MOI of 10 and analyzed at 4 h post-infection. (I) Western blot analysis and relative intensity of *p*-FOXO3A (Ser253) and FOXO3A (n = 4 independent experiments). (J) Western blot analysis and relative intensity of *p*-AKT (Ser473) and AKT (n = 4 independent experiments). (K) HEK293T cells were transfected with Flag-AKT together with either an empty vector or GFP-NLRP6 (left), or transfected with combinations of GFP-NLRP6 and Flag-AKT or its empty vector (right) for 48 h. Coimmunoprecipitation of AKT and NLRP6. (L–N) BMDMs isolated from wild-type and *Nlrp6*$^{-/-}$ mice were treated with either vehicle or 1 μM MK2206 for 2 h and then infected with *S*. Typhimurium strain SL1344 at an MOI of 10 for 4 h. (L) Non-heme iron content in BMDMs (n = 4 independent experiments). (M) Quantitative PCR analysis of *Fpn*, *Nqo1* and *Keap1* (n = 4 independent experiments). (N) Western blot analysis and relative intensity of *p*-FOXO3A (Ser253), FOXO3A, p-p62 (Ser351), *p*-AKT (Ser473) and AKT (n = 4 independent experiments). Data were compared with independent Student's *t*-test. Values are expressed as the mean ± SEM, and statistically significant differences are indicated. *$P < 0.05$; **$P < 0.01$; ns, not significant.

It has been reported that bacteria have evolved several mechanisms to obtain the iron necessary to satisfy their metabolic demand, which result in hypoferremia and tissue iron overload. For example, previous study from other laboratory demonstrated that *entC*, *sit*, and *feo* are three major iron uptake systems of *S*. Typhimurium [34]; we recently reported that *S*. Typhimurium secreted the pSLT-encoded cytotoxic effector SpvB to scavenge iron from the host by interfering with both cellular and systemic iron metabolisms [9,13]. Therefore, a growing body of evidence suggests that limiting bacterial iron acquisition is meaningful to maintain host physiological iron homeostasis and control bacteria growth [6]. Although a previous study showed that a transmembrane-associated PRRs toll-like receptor 4 (TLR4) could modulate iron metabolism response to bacterial pathogens [35], the precise role of cytosolic PRRs in this essential component of the nutritional immunity remained to be elucidated. In the present study, our results demonstrate that NLRP6 plays a detrimental role in maintaining host iron homeostasis during infection. Macrophage iron sequestration affects the trafficking of iron in the body and results in hypoferremia [36]. Therefore, the principal manifestation of S. Typhimurium-induced iron metabolic dysregulation is a reduction in serum iron content and an accumulation of iron in systemic organs [9,10]. In line with previous works from our laboratory and another, the data presented in Fig. 1E and F indicated that the infected wild-type mice exhibited severe hypoferremia and markedly iron accumulation in spleen. Importantly, NLRP6 deficiency efficiently alleviates hypoferremia and decreases splenic iron overload, suggesting that downregulation of NLRP6 could be advantageous for ameliorating iron metabolic disorder during S. Typhimurium infection. Of interest, loss of NLRP6 alters non-heme iron content but has no apparent effects on heme levels, and these changes occur in hepatic macrophages rather than hepatocytes. It is therefore possible that NLRP6 is involved in the regulation of iron recycling. We confirmed this hypothesis both *in vitro* and *in vivo* through knockdown of either FPN or NRF2. Our data showed that NLRP6 deficiency caused a significantly higher expression of FPN and mediated an increase of iron export in macrophages in a KEAP1/NRF2 pathway-dependent manner. Inhibition of NRF2 resulted in a reduction of FPN accumulation, aggravated disorders in iron homeostasis, and increased tissue bacterial burden in *S*. Typhimurium-infected *Nlrp6*$^{-/-}$ mice.

NRF2 abundance and activation within the cell is tightly regulated by KEAP1, which directly binds to NRF2 and prevents its nuclear translocation [37]. Given that the present study did not detect any significant influence of NLRP6 on NRF2 transcription, we focused on elucidating potential NLRP6 impacts on KEAP1/NRF2 interaction. It has been reported that the autophagy receptor protein p62 functions as a positive regulator of NRF2 by facilitating KEAP1 dissociation from the NRF2/KEAP1 complex and inducing autophagic degradation of KEAP1 [38,39]. As an extension of a previous study where Wlodarska et al. showed that NLRP6 affected autophagy in goblet cells [28], we found that NLRP6 deficiency also resulted in a decrease of autophagic flux in macrophages. Our data further indicated that p62 and NDP52, but not the other three autophagic receptors tested, were involved in NLRP6-induced autophagy during *S*. Typhimurium infection. Thus, these results suggest that NLRP6 inhibited NRF2 activity by enhancing KEAP1/NRF2 interaction rather than reducing KEAP1 autophagic degradation. This study further revealed that NLRP6 deficiency contributes to a higher level of phosphorylation on Ser351 of p62 during *S*. Typhimurium infection. Although suppressing mTORC1 activity reversed the effect of NLRP6 on p62 phosphorylation, it is interesting to note that a mTORC1 inhibitor had a smaller reducing effect on NRF2 activation. Previous study from Ichimura et al. implied that (an)other kinase(s) may participate in p62 phosphorylation at Ser351 [21]. The data from our present study support one possible explanation for this phenomenon. That is, mTORC1 inhibition could induce elevated phosphorylation of AKT, which subsequently may lead to a decrease in KEAP1 transcription through inhibition of the FOXO3A pathway. Our *in vitro* and *in vivo* experiments provide additional evidence supporting that NLRP6-mediated suppression of AKT activation aggravates the dysregulation of iron metabolism caused by infection and promotes *S*. Typhimurium survival.

In addition to liver and macrophages, duodenum and enterocytes play important roles in the absorption of dietary iron [40]. Our data showed that accumulation of NRF2 and FPN during *S*. Typhimurium infection occurs not only in NLRP6-deficient liver and macrophages but also in NLRP6-deficient duodenum and Caco-2 cells. It is noteworthy that the changes in AKT activity, autophagic flux, and iron burden caused by NLRP6 deficiency were also found in Caco-2 cells. These observations indicate that the molecular mechanism underlying the regulation of FPN by NLRP6 in macrophages is also required for intestinal iron absorption.

In summary, by functionally characterizing the role of NLRP6 in the transcriptional regulation of the cellular iron exporter FPN during *S*. Typhimurium infection, we provide new insights into the mechanisms of nutritional immunity in which cytoplasmic PRRs have a fundamental effect on modulating iron metabolism. These findings reveal a novel mechanism whereby NLRP6-mediated posttranslational modification of AKT phosphorylation regulates iron homeostasis *via* KEAP1/NRF2 pathway inhibition and subsequent transcriptional downregulation of FPN. While we demonstrated that NLRP6, belonging to the NLRs family, is a regulator of iron metabolism, it remains to be seen if other NLRs also contribute to nutritional immunity during infection.

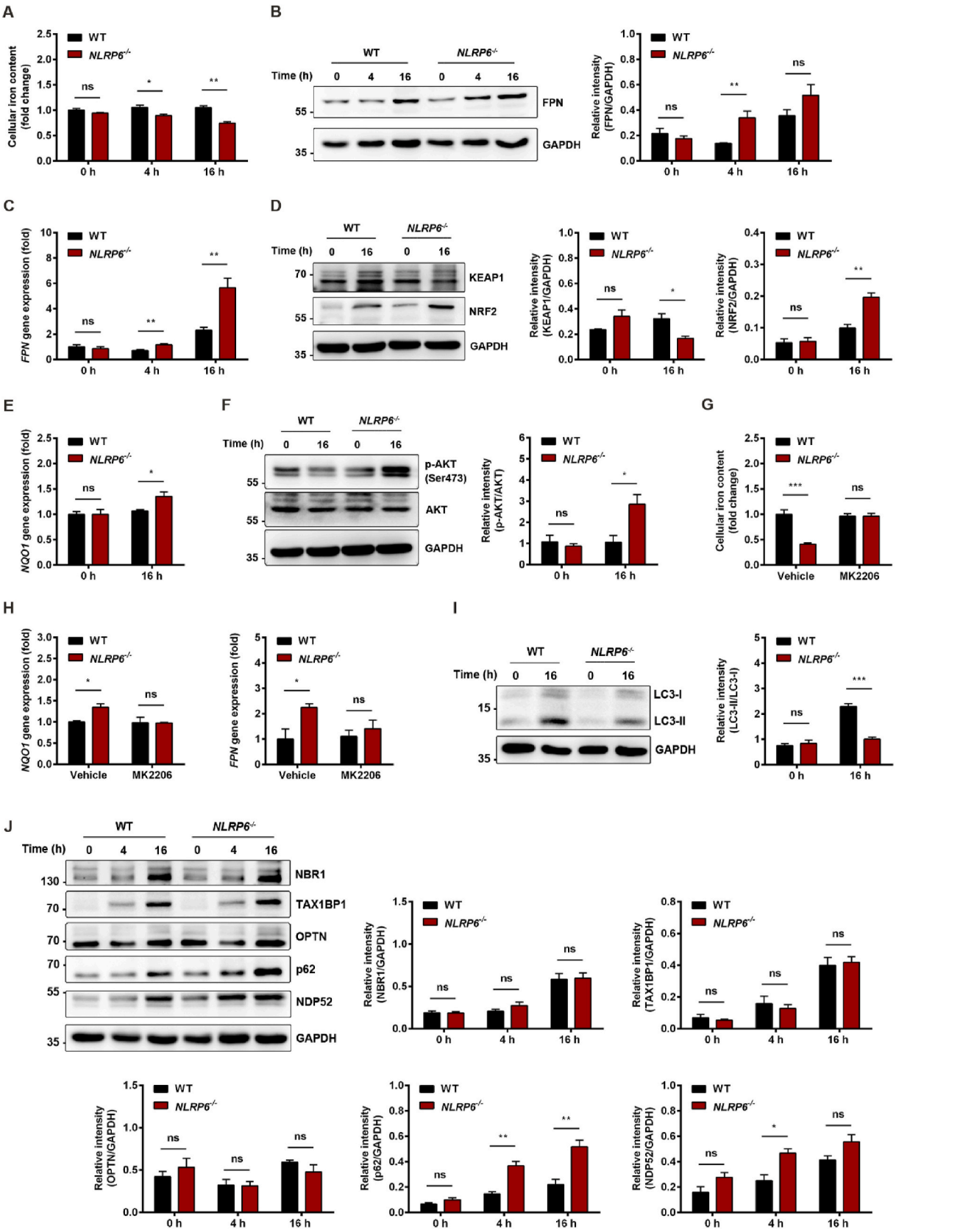

(caption on next page)

Fig. 6. NLRP6 interferes with enterocyte iron metabolism upon *S*. Typhimurium infection. (A–F) Wild-type and *NLRP6*$^{-/-}$ Caco-2 cells were infected with *S*. Typhimurium strain SL1344 at an MOI of 50 for the indicated time points. (A) Non-heme iron content in Caco-2 cells (n = 4 independent experiments). (B) Western blot analysis and relative intensity of FPN (n = 4 independent experiments). (C) Quantitative PCR analysis of *FPN* (n = 4 independent experiments). (D) Western blot analysis and relative intensity of KEAP1 and NRF2 (n = 4 independent experiments). (E) Quantitative PCR analysis of *NQO1* (n = 4 independent experiments). (F) Western blot analysis and relative intensity of *p*-AKT (Ser473) and AKT (n = 4 independent experiments). (G, H) Wild-type and *NLRP6*$^{-/-}$ Caco-2 cells were treated with either vehicle or 1 μM MK2206 for 2 h and then infected with *S*. Typhimurium strain SL1344 at an MOI of 50 for 16 h. (G) Non-heme iron content in Caco-2 cells (n = 4 independent experiments). (H) Quantitative PCR analysis of *NQO1* and *FPN* (n = 4 independent experiments). (I, J) Wild-type and *NLRP6*$^{-/-}$ Caco-2 cells were infected with *S*. Typhimurium strain SL1344 at an MOI of 50 for the indicated time points. (I) Western blot analysis and relative intensity of LC3 (n = 4 independent experiments). (J) Western blot analysis and relative intensity of NBR1, TAX1BP1, OPTN, p62 and NDP52 (n = 4 independent experiments). Data were compared with independent Student's *t*-test. Values are expressed as the mean ± SEM, and statistically significant differences are indicated. $^{*}P < 0.05$; $^{**}P < 0.01$; $^{***}P < 0.001$; ns, not significant.

4. Materials and methods

4.1. Animals and ethics statement

Wild-type C57BL/6 mice were obtained from the experimental animal center of Soochow University. *Nlrp6* knockout mice (*Nlrp6*$^{-/-}$), on the C57BL/6 genetic background, were a gift from Professor Ying Xu (Cambridge-Suda Genome Resource Center, Soochow University, Suzhou, China). Female wild-type and *Nlrp6*$^{-/-}$ mice were bred in ventilated cages under 12-h light/dark cycles in specific pathogen-free conditions and received sterile water and food *ad libitum*. Before the start of the study, the *Nlrp6*$^{-/-}$ mice had been backcrossed for at least eight generations with wild-type C57BL/6 mice. The experiments were performed on 10-12-week-old animals. All of the animal experiments were conducted in accordance with the principles and procedures outlined in the National Institutes of Health Guidelines for the Care and Use of Laboratory Animals (NIH Guidelines) and were approved by the Animal Experimental Committee of Soochow University (Grant 2111270).

4.2. Bacterial strain and growth conditions

Wild-type *S.* Typhimurium strain SL1344 was a gift from Professor Qian Yang (Nanjing Agricultural University, Nanjing, China) and used for all experiments in this study. SL1344 was grown under sterile conditions on Luria-Bertani (LB) agar (Hangwei, Hangzhou, China) plates or in LB medium (Hangwei). On the day of experiments, overnight bacteria cultures were diluted in a ratio of 1:100 and agitated for a further another 3 h until reaching the late-logarithmic phase. Upon washing 3 times with sterile PBS (Sangon Biotech, Shanghai, China), numbers of *S*. Typhimurium in fresh bacterial suspension were estimated and adjusted based on the optical density at 600 nm absorbance and ready for the infection experiment.

4.3. S. Typhimurium infection in vivo

For *in vivo* experiments, *S*. Typhimurium was resuspended in sterile 0.9% NaCl. Mice pretreated with 20 mg/mouse streptomycin (Sangon Biotech) for 24 h were orally gavage with 1×10^7 colony-forming units (CFUs) of SL1344. To investigate the role of NRF2 in NLRP6-associated regulation of iron metabolism, mice were intravenously injected with 1×10^8 transducing unit (TU) of either control lentivirus or a lentivirus expressing Nrf2 shRNA (GenePharma, Shanghai, China) for 10 days before administrating with streptomycin. To investigate the role of AKT in NLRP6-associated regulation of iron metabolism, mice were orally gavage with either vehicle or 120 mg/kg MK2206 (MCE, New Jersey, USA) at 1 day post-infection. To determine the viable counts of *S*. Typhimurium, tissues were harvested, weighed, mechanically homogenized in sterile 0.5% (vol/vol) Tergitol (MilliporeSigma, Burlington, MA, USA) supplemented with 0.5% (vol/vol) heat-inactivated fetal bovine serum (FBS; Biological Industries, Kibbutz Beit-Haemek, Israel). The bacterial burden of organs was determined by plating homogenized tissues in appropriate dilutions on *Salmonella-Shigella* agar plates (Hangwei) and the number of bacteria was calculated per gram of tissue wet weight as previously described [7].

4.4. Isolation of mouse hepatocytes, non-parenchymal liver cells, and liver macrophages

Hepatocytes, non-parenchymal liver cells and liver macrophages were isolated as previously described with minor modifications [9,41]. In brief, livers were harvested, perfused with calcium and magnesium-free Hank's Balanced Salt Solution (HBSS; Beyotime Biotechnology, Shanghai, China) and digested with collagenase type I (Worthington, Lakewood, NJ, USA). The dissociated cells were filtered through a 70 μm cell strainer (Sorfa, Zhejiang, China) and then centrifuged at 50 *g* for 5 min at 4 °C. The hepatocyte pellets were collected and processed to eliminate erythrocyte using the Red Blood Cell Lysis Buffer (Beyotime Biotechnology). The supernatant fluids were transferred to a clean collection tube and centrifuged at 500 *g* for 10 min at 4 °C. The non-parenchymal liver cell pellets were collected and processed to eliminate erythrocyte using the Red Blood Cell Lysis Buffer (Beyotime Biotechnology). Liver macrophages were isolated from the non-parenchymal liver cell fraction as previously described with minor modifications [42]. Briefly, the non-parenchymal liver cell pellets were resuspended in sterile PBS (Sangon Biotech), gently layered on a double Percoll gradient (25% and 50%; GE Healthcare, Buckinghamshire, UK), and centrifuged at 900 *g* for 20 min at 4 °C. The layer between the 25%–50% gradient interface was collected.

4.5. Cell culture

Bone marrow from wild-type C57BL/6 mice and *Nlrp6* knockout mice was maintained in RPMI medium (HyClone Laboratories, Logan, UT, USA) supplemented with 10% (vol/vol) heat-inactivated FBS (Biological Industries), 10 ng/ml of Macrophage Colony Stimulating Factor (M-CSF; PeproTech, Rocky Hill, NJ, USA) and 1% (vol/vol) penicillin-streptomycin (Beyotime Biotechnology). Nonadherent cells were removed on day 3. Cells became mature bone marrow derived macrophages (BMDMs) on day 7, and adherent BMDMs were collected to conduct subsequent experiments. Mouse embryonic fibroblasts (MEFs) isolated from wild-type C57BL/6 mice and *Nlrp6* knockout mice were grown in Dulbecco's Modified Eagle Medium (DMEM; HyClone Laboratories, Logan, UT, USA) containing 10% (vol/vol) heat-inactivated FBS (Biological Industries) and 1% (vol/vol) penicillin-streptomycin (Beyotime Biotechnology). Caco-2 cells (human colon carcinoma cell line) were a gift from Professor Weiqi He (Cambridge Suda Genome Resource Center, Soochow University, Suzhou, China). *NLRP6* knockout (*NLRP6*$^{-/-}$) Caco-2 cells were constructed using the clustered regularly interspaced short palindromic repeats (CRISPR)/CRISPR-associated protein 9 (Cas9) gene editing system as previously described [13,43]. THP-1 cells (human monocytic cell line), HeLa cells (human epithelial carcinoma cell line) and HEK293T cells (human embryonic kidney cell line) were purchased from the American Type Culture Collection (ATCC; Manassas, VA, USA). THP-1 cells were grown in Roswell Park Memorial Institute (RPMI) 1640 medium (HyClone Laboratories) containing 10% (vol/vol) heat-inactivated FBS (Biological Industries). THP-1 cells were differentiated into adherent macrophage-like cells by 100 nM phorbol 12-myristate 13-acetate (PMA; MilliporeSigma) for 48 h. HeLa cells and HEK293T cells were grown in DMEM medium (HyClone Laboratories)

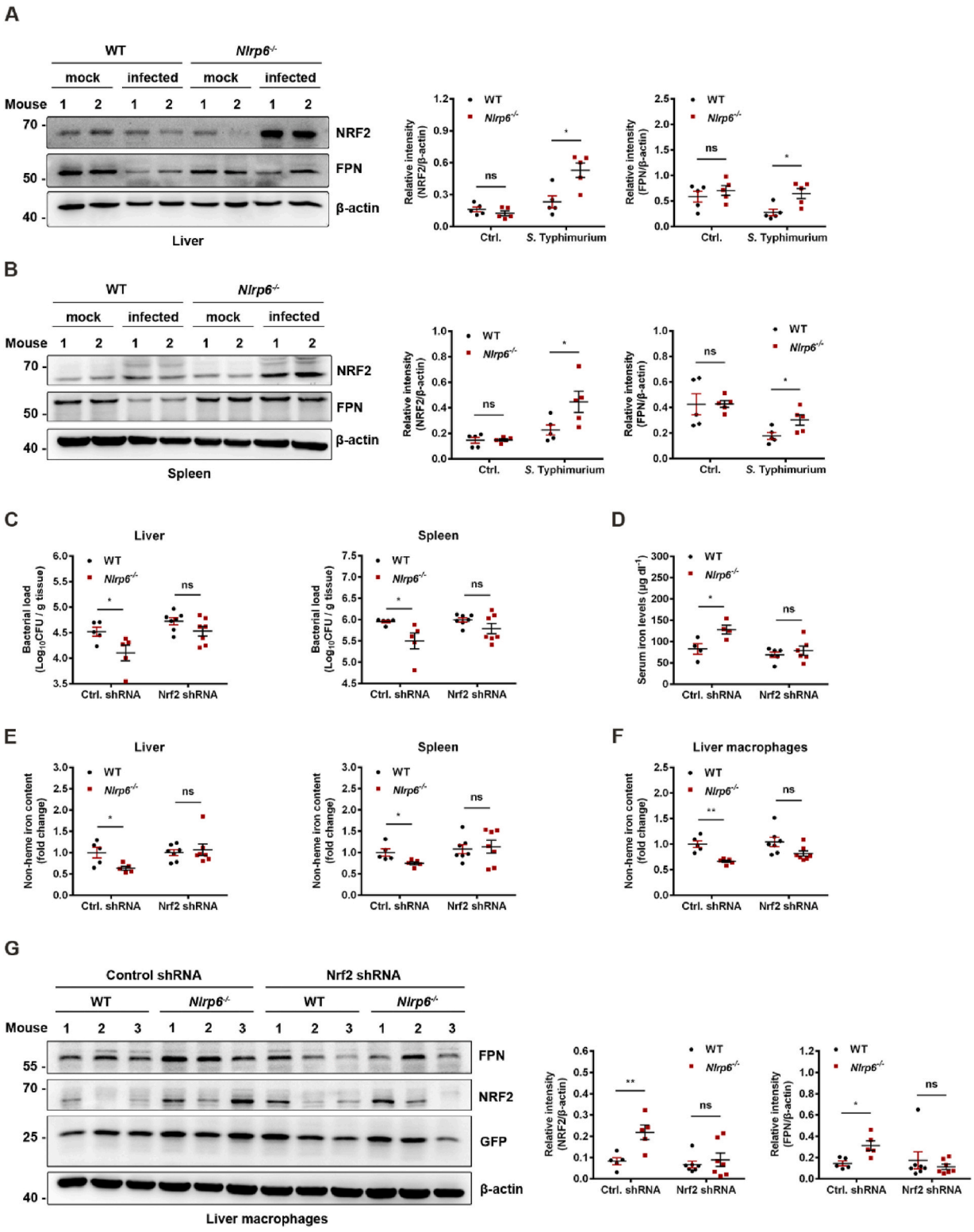

Fig. 7. NLRP6 regulates FPN expression and disturbs iron homeostasis through NRF2 pathway *in vivo*. (A, B) Streptomycin-pretreated wild-type and *Nlrp6*$^{-/-}$ mice were orally infected with 1×10^7 CFUs of *S*. Typhimurium strain SL1344 and analyzed at 3 days post-infection. (A) Western blot analysis and relative intensity of NRF2 and FPN in liver (n = 5 per group). (B) Western blot analysis and relative intensity of NRF2 and FPN in spleen (n = 5 per group). (C–G) Wild-type and *Nlrp6*$^{-/-}$ mice were intravenously injected with 1×10^8 TU of either control lentivirus or a lentivirus expressing Nrf2 shRNA. After 10 days of pretreatment, wild-type and *Nlrp6*$^{-/-}$ mice were orally administrated with 20 mg streptomycin for 24 h and infected with 1×10^7 CFUs of *S*. Typhimurium strain SL1344 for 3 days. (C) Viable count of *S*. Typhimurium in liver and spleen (Ctrl. shRNA, n = 5 per group; Nrf2 shRNA, n = 7 per group). (D) Serum iron levels (Ctrl. shRNA, n = 5 per group; Nrf2 shRNA, n = 7 per group). (E) Non-heme iron content in liver and spleen (Ctrl. shRNA, n = 5 per group; Nrf2 shRNA, n = 7 per group). (F) Non-heme iron content in isolated liver macrophages (Ctrl. shRNA, n = 5 per group; Nrf2 shRNA, n = 7 per group). (G) Western blot analysis and relative intensity of NRF2 and FPN in isolated liver macrophages (Ctrl. shRNA, n = 5 per group; Nrf2 shRNA, n = 7 per group). Data were compared with independent Student's *t*-test. Values are expressed as the mean ± SEM, and statistically significant differences are indicated. *$P < 0.05$; **$P < 0.01$; ns, not significant.

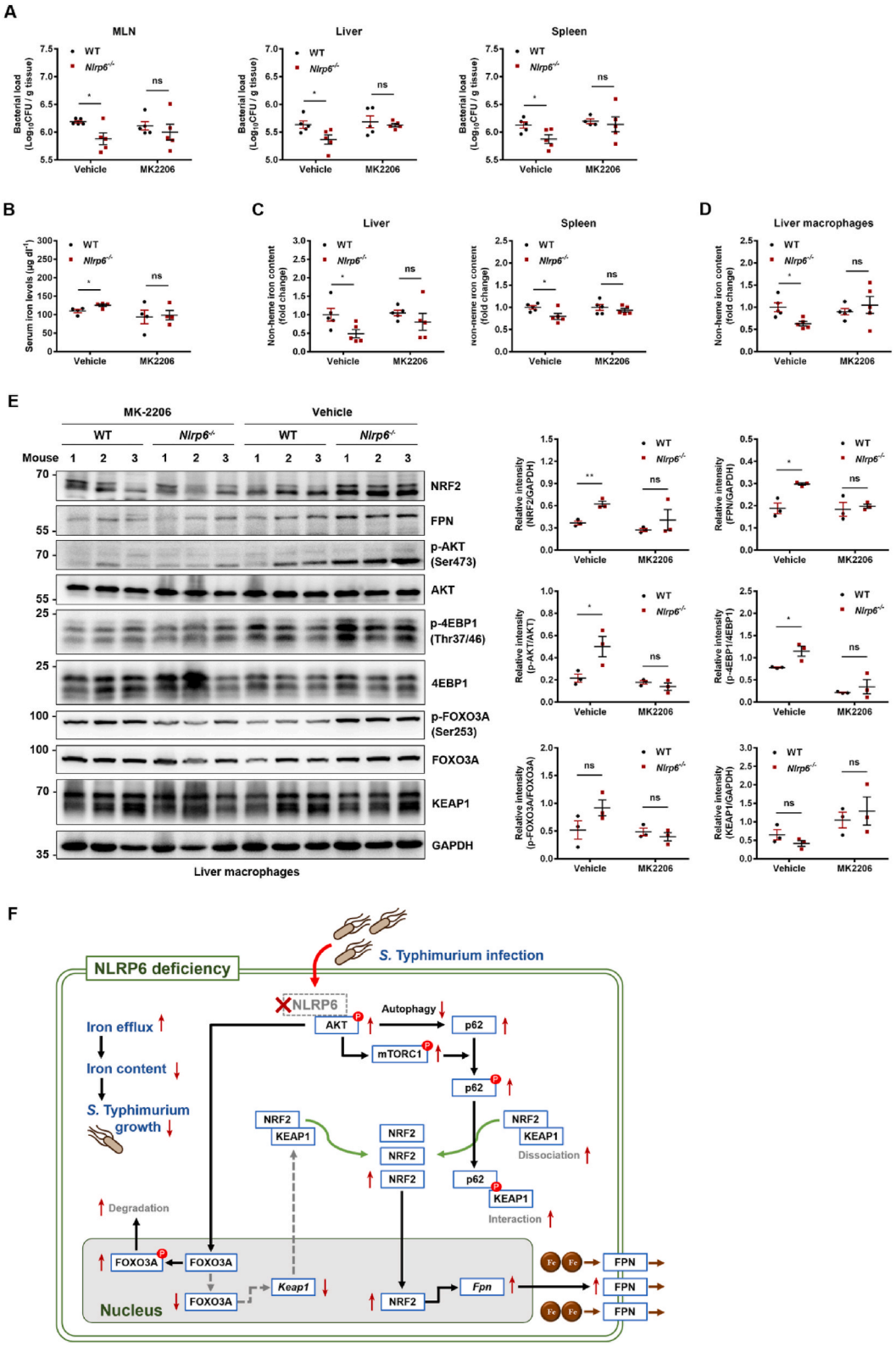

Fig. 8. The changes in host iron metabolism and antimicrobial defense resulting from *Nlrp6*-deficiency are reversed by pharmacological inhibition of AKT *in vivo*. Streptomycin-pretreated wild-type and *Nlrp6*$^{-/-}$ mice were orally infected with 1×10^7 CFUs of *S.* Typhimurium strain SL1344. After 1 day of infection, mice were orally administrated with either vehicle or 120 mg/kg MK2206 and analyzed 3 days post-infection. (A) Viable count of *S.* Typhimurium in MLN, liver and spleen (n = 4–5 per group). (B) Serum iron levels (n = 4 per group). (C) Non-heme iron content in liver and spleen (n = 5 per group). (D) Non-heme iron content in isolated liver macrophages (n = 5 per group). (E) Western blot analysis and relative intensity of NRF2, FPN, *p*-AKT (Ser473), AKT, p-4EBP1 (Thr37/46), 4EBP1, *p*-FOXO3A (Ser253), FOXO3A and KEAP1 (n = 3 per group). (F) Model of NLRP6 in regulating host iron metabolism during *S.* Typhimurium infection. Data were compared with independent Student's *t*-test. Values are expressed as the mean ± SEM, and statistically significant differences are indicated. *$P < 0.05$; **$P < 0.01$; ns, not significant.

containing 10% (vol/vol) heat-inactivated FBS (Biological Industries).

4.6. Plasmid, siRNA and transfection experiments

Plasmid RFP-GFP-LC3 was a gift from Professor Tamotsu Yoshimori (Osaka University, Osaka, Japan). The Cas9 expression plasmid pST1374-Cas9-N-NLS-Flag linker, the single guide RNA (sgRNA) plasmid pGL3-U6-sgRNA-PGKPuro and plasmid pPBB-EF-EGFP-C were gifts from Professor Ying Xu (Cambridge Suda Genome Resource Center, Soochow University, Suzhou, China). Plasmid pCMV-HA, pcDNA3.1-Flag and pcDNA3.1-Flag-AKT were purchased from Public Protein/Plasmid Library (PPL). A fragment of His-NLRP6 was cloned into pCMV-HA or pPBB-EF-EGFP-C. THP-1 macrophages were transiently transfected with plasmid using Lipofectamine 3000 (Thermo Fisher Scientific, Waltham, MA, USA) for 48 h according to the manufacturer's instructions. HeLa cells were transiently transfected with plasmid using Lipofectamine 2000 (Thermo Fisher Scientific) for 36 h according to the manufacturer's instructions. The negative control siRNA (NC siRNA) and siRNA specific for Fpn, Arnt, Mtf1 or Nrf2 were purchased from GenePharma. BMDMs and MEFs were transfected with 50 nM siRNA using Lipofectamine RNAiMAX reagent (Thermo Fisher Scientific) for 48 h according to the manufacturer's instructions. Knockdown efficiency was assessed by quantitative PCR.

4.7. S. Typhimurium infection in vitro

For *in vitro* experiments, *S*. Typhimurium was resuspended in RPMI medium (HyClone Laboratories) or DMEM medium (HyClone Laboratories) without FBS and added to mammalian cells at a multiplicity of infection (MOI) as described in the figure legends. BMDMs were washed 3 times with sterile PBS (Sangon Biotech) at 30 min after infection and other cells were washed at 1 h post-infection to remove extracellular bacteria. Infected cells were subsequently cultured in RPMI medium or DMEM medium containing 10% (vol/vol) heat-inactivated FBS (Biological Industries) and 50 μg/ml gentamicin (Sangon Biotech) for 2 h. Afterward, cell culture medium was replaced with those containing 10% (vol/vol) FBS (Biological Industries) and 10 μg/ml gentamicin (Sangon Biotech). Samples were collected for further experiments at the indicated time points as described in the figure legends. When appropriate, cells were pre-treated or treated with 50 μM deferiprone (DFP; MilliporeSigma), 5 μM actinomycin D (MCE), 200 nM bafilomycin A1 (BafA1; MCE), 1 μM rapamycin (MCE) and 1 μM MK2206 (MCE) for indicated times as described in the figure legends. To determine intracellular bacteria loads, cells were washed 5 times with sterile PBS (Sangon Biotech), lysed in 1 ml 0.3% (vol/vol) Triton X-100 (MilliporeSigma), and subsequently plated in appropriate dilutions on LB agar plates (Hangwei). Adhesion and invasion assays were performed as previously described [44].

4.8. Histopathology and Perls' Prussian Blue staining

Duodenum, colon, liver and spleen samples were fixed in 4% paraformaldehyde (Servicebio, Wuhan, China), embedded in paraffin and cut into 5-μm thick sections. The sections were then subjected to hematoxylin-eosin staining (Servicebio) or Perls' Prussian Blue staining (Servicebio) according to the manufacturer's instructions. Scores for pathology were analyzed according to the methods described previously [45–47]. Photomicrographs were taken with a Nikon Eclipse Ni–U fluorescence microscope (Nikon Corporation, Tokyo, Japan) with NIS-Elements F (Nikon Corporation).

4.9. Non-heme and heme iron assays

Non-heme and heme iron assays were performed as previously described [48]. In brief, blood samples were collected from anesthetized mice through intracardiac puncture. Tissue and cell samples were lysed in RIPA Lysis Buffer (Beyotime Biotechnology), and protein concentrations were measured using the BCA Protein Assay (Beyotime Biotechnology). Detection of non-heme iron content was measured using an iron assay kit (BioAssay Systems, Hayward, CA, USA) according to the manufacturer's instructions and normalized to the protein concentration of each sample. Calculation of iron release was performed as previously described [49]. To determine heme levels, equal amounts of samples were mixed with 2 M oxalic acid (Meilunbio, Beijing, China), heated to 95 °C for 30 min, and then centrifuged at 1000 *g* for 10 min at 4 °C to remove debris. The fluorescence of the supernatant was assessed on the Synergy 2 Multiscan Spectrum (BioTek, Vermont, USA) and normalized to the protein concentration of each sample.

4.10. RNA isolation and quantitative PCR

Total RNA was isolated using TRIzol reagent (Beyotime Biotechnology) and reverse-transcribed using the All-in-one RT MasterMix kit (Applied Biological Materials, Richmond, BC, Canada) according to the manufacturer's instructions. The transcript levels of different genes were analyzed using EvaGreen MasterMix-Low ROX (Applied Biological Materials) on the ViiA7 real-time PCR instrument (Applied Biosystems, Carlsbad, CA, USA) according to the manufacturer's instructions. Targeted genes were amplified with specific primers as previously described [9,20,27,50]. Results were normalized to the housekeeping gene *Gapdh* or *β-ACTIN* measured in the same samples and expressed as fold induction in comparison to baseline levels, which were set at a value of 1.

4.11. Western blot analysis

Samples were lysed in RIPA Lysis Buffer (Beyotime Biotechnology) containing protease and phosphatase inhibitor (Beyotime Biotechnology). Protein concentrations were measured using the BCA Protein Assay (Beyotime Biotechnology). Equal amounts of cell lysates were separated on SDS-PAGE and electroblotted onto PVDF membranes (MilliporeSigma, Burlington, MA, USA). Membranes were incubated with 5% nonfat dry milk powder in TBST containing 0.1% Tween 20 at room temperature for 1 h to block nonspecific binding, and then probed with the corresponding primary antibodies at 4 °C overnight. After incubating with the appropriate horseradish peroxidase–labeled secondary antibodies at room temperature for 1 h, membranes were then visualized with an enhanced chemiluminescence luminescence reagent (Meilunbio). The intensities of the bands were calculated by ImageJ Launcher broken symmetry software program (NIH, Bethesda, MD, USA). Primary antibodies to FPN (NBP1-21502) and LC3 (NBP100-2220) were purchased from Novus Biologicals (Littleton, CO, USA). Primary antibodies to *p*-AKT (Ser473; #9271), AKT (#4691), p-4EBP1 (Thr37/46; #2855), 4EBP1 (#9644), p62 (#5114) and ATG16L1 (#8089) were purchased from Cell Signaling Technology (Danvers, MA, USA). Primary antibodies to NDP52 (12229-1-AP), OPTN (10837-1-AP), TAX1BP1 (14424-1-AP), NBR1 (16004-1-AP), KEAP1 (10503-2-AP) and FOXO3A (10849-1-AP) were purchased from Proteintech (Rosemont, IL, USA). Primary antibodies to p-p62 (Ser349; ab211324), NRF2 (ab31163), *p*-FOXO3A (Ser253; ab154786), FTL (ab109373), FTH (ab183781), ubiquitin K63 (ab179434) and ATG5 (ab108327) were purchased from Abcam (Cambridge, MA, USA). Primary antibodies to NLRP6 (SAB1302240), β-actin (SAB1305554) and GFP (SAB4301138) were purchased from Sigma-Aldrich (St. Louis, MO, USA). Primary antibodies to FLAG (MA1-91878) and 6 × His (MA1-21315) were purchased from Thermo Fisher Scientific. Primary antibody to GAPDH (bs-10900R) was purchased from Boster Biological Technology (Beijing, China).

4.12. Immunofluorescence

Cells were seeded on glass coverslips and incubated with *S*. Typhimurium described in the figure legends. After being washed 3 times with

sterile PBS (Sangon Biotech), the samples were fixed with 4% paraformaldehyde (Servicebio) at room temperature for 20 min and incubated with 0.3% (vol/vol) Triton X-100 (MilliporeSigma) for 10 min. After being blocked with 3% bovine serum albumin (BSA; Beyotime Biotechnology), the samples were incubated with primary antibodies at 4 °C overnight, developed with the appropriate Alexa Fluor® 555 secondary antibody (Thermo Fisher Scientific) at room temperature for 1 h, and then incubated with DAPI (Sigma-Aldrich) for 10 min. Photomicrographs were taken with a Nikon Eclipse Ni–U fluorescence microscope (Nikon Corporation, Tokyo, Japan) with NIS-Elements F (Nikon Corporation). Primary antibody to NRF2 (ab31163) was purchased from Abcam (Cambridge, MA, USA). Primary antibody to FOXO3A (10849-1-AP) was purchased from Proteintech (Rosemont, IL, USA).

4.13. Luciferase reporter assay

A fragment of the human *KEAP1* promoter was cloned into the pGL3-basic luciferase reporter gene vector (Promega, Madison, WI, USA). Promoter activity was measured using the Dual Luciferase assay kit (Promega) according to the manufacturer's instructions. Firefly luciferase activity was corrected by co-transfection of cells with the constitutively expressed Renilla luciferase vector phRL-TK (Clontech, Mountain View, CA, USA).

4.14. Immunoprecipitation

Samples were lysed in NP-40 Lysis Buffer (Beyotime Biotechnology) containing protease and phosphatase inhibitor (Beyotime Biotechnology). Cell lysates were collected and incubated with protein A/G Plus-Agarose (Santa Cruz Biotechnology, Dallas, TX, USA) at 4 °C for 4 h. The suspension was then incubated with the corresponding primary antibodies together with protein A/G Plus-Agarose (Santa Cruz Biotechnology) at 4 °C overnight. Agarose were then washed five times with NP-40 Lysis Buffer (Beyotime Biotechnology) and prepared for Western blot analysis. When appropriate, cells were treated with 10 μM MG-132 (Selleck Chemicals, Houston, TX, USA).

4.15. Statistical analysis

Data are presented as mean ± SEM. Statistical analysis was performed using IBM SPSS statistics 22 (Chicago, IL, USA). Survival rates were estimated by the Gehan-Breslow-Wilcoxon test. Normality of numerical variables was assessed and in the case of normality, an independent Student's *t*-test was applied for comparisons of 2 groups. Values of $P < 0.05$ were considered statistically significant.

Funding

The work is supported by National Natural Science Foundation of China (No. 81971899, No. 31970132), Suzhou Municipal Science and Technology Foundation (SYS2019031), Project funded by China Postdoctoral Science Foundation (2021M693668) and a project funded by the Priority Academic Program Development (PAPD) of Jiangsu Higher Education Institutions.

Author contributions

Q. Deng, S. Yang, and R. Huang designed the research; Q. Deng, S. Yang, and K. Huang contributed to development of methodology and interpretation of data; Q. Deng, S. Yang, L. Sun, K. Dong, Y. Zhu, Y. Cao and Y. Li performed the experiments; Q. Deng, and S. Yang prepared figures and wrote the manuscript; L. Sun, S. Wu, and R. Huang edited the manuscript; R. Huang supervised the project.

Declaration of competing interest

The authors declare no conflicts of interest.

Acknowledgements

The authors thank Professor Ying Xu (Cambridge-Suda Genome Resource Center, Soochow University, Suzhou, China) for providing excellent technical assistance and her helpful discussion, Ying Ye (Cambridge-Suda Genome Resource Center, Soochow University, Suzhou, China) for isolation of mouse embryonic fibroblasts, Lei Liu (School of Biology & Basic Medical Sciences, Medical College of Soochow University, Suzhou, China) and Peng Wang (School of Public Health, Medical College of Soochow University, Suzhou, China) for intravenously administration of shRNA and isolation of liver macrophages.

Appendix A. Supplementary data

Supplementary data to this article can be found online at https://doi.org/10.1016/j.redox.2021.102217.

References

[1] M.I. Hood, E.P. Skaar, Nutritional immunity: transition metals at the pathogen-host interface, Nat. Rev. Microbiol. 10 (2012) 525–537.
[2] J.E. Cassat, E.P. Skaar, Iron in infection and immunity, Cell Host Microbe 13 (2013) 509–519.
[3] A. Sousa Geros, A. Simmons, H. Drakesmith, A. Aulicino, J.N. Frost, The battle for iron in enteric infections, Immunology 161 (2020) 186–199.
[4] M.W. Hentze, M.U. Muckenthaler, B. Galy, C. Camaschella, Two to tango: regulation of Mammalian iron metabolism, Cell 142 (2010) 24–38.
[5] A. Katsarou, K. Pantopoulos, Basics and principles of cellular and systemic iron homeostasis, Mol. Aspect. Med. 75 (2020) 100866.
[6] H. Drakesmith, E. Nemeth, T. Ganz, Ironing out ferroportin, Cell Metabol. 22 (2015) 777–787.
[7] M. Nairz, U. Schleicher, A. Schroll, T. Sonnweber, I. Theurl, S. Ludwiczek, H. Talasz, G. Brandacher, P.L. Moser, M.U. Muckenthaler, F.C. Fang, C. Bogdan, G. Weiss, Nitric oxide-mediated regulation of ferroportin-1 controls macrophage iron homeostasis and immune function in Salmonella infection, J. Exp. Med. 210 (2013) 855–873.
[8] C.D. Camell, P. Gunther, A. Lee, E.L. Goldberg, O. Spadaro, Y.H. Youm, A. Bartke, G.B. Hubbard, Y. Ikeno, N.H. Ruddle, J. Schultze, V.D. Dixit, Aging induces an Nlrp3 inflammasome-dependent expansion of adipose B cells that impairs metabolic homeostasis, Cell Metabol. 30 (2019) 1024–1039 e1026.
[9] Q. Deng, S. Yang, L. Sun, K. Dong, Y. Li, S. Wu, R. Huang, Salmonella effector SpvB aggravates dysregulation of systemic iron metabolism via modulating the hepcidin-ferroportin axis, Gut Microb. 13 (2021) 1–18.
[10] D.K. Kim, J.H. Jeong, J.M. Lee, K.S. Kim, S.H. Park, Y.D. Kim, M. Koh, M. Shin, Y. S. Jung, H.S. Kim, T.H. Lee, B.C. Oh, J.I. Kim, H.T. Park, W.I. Jeong, C.H. Lee, S. B. Park, J.J. Min, S.I. Jung, S.Y. Choi, H.E. Choy, H.S. Choi, Inverse agonist of estrogen-related receptor gamma controls Salmonella typhimurium infection by modulating host iron homeostasis, Nat. Med. 20 (2014) 419–424.
[11] J. Behnsen, A. Perez-Lopez, S.P. Nuccio, M. Raffatellu, Exploiting host immunity: the Salmonella paradigm, Trends Immunol. 36 (2015) 112–120.
[12] N.C. Winn, K.M. Volk, A.H. Hasty, Regulation of tissue iron homeostasis: the macrophage "ferrostat, JCI insight 5 (2020).
[13] S. Yang, Q. Deng, L. Sun, K. Dong, Y. Li, S. Wu, R. Huang, Salmonella effector SpvB interferes with intracellular iron homeostasis via regulation of transcription factor NRF2, Faseb. J. 33 (2019) 13450–13464.
[14] N. Harada, M. Kanayama, A. Maruyama, A. Yoshida, K. Tazumi, T. Hosoya, J. Mimura, T. Toki, J.M. Maher, M. Yamamoto, K. Itoh, Nrf2 regulates ferroportin 1-mediated iron efflux and counteracts lipopolysaccharide-induced ferroportin 1 mRNA suppression in macrophages, Arch. Biochem. Biophys. 508 (2011) 101–109.
[15] M. Taylor, A. Qu, E.R. Anderson, T. Matsubara, A. Martin, F.J. Gonzalez, Y. M. Shah, Hypoxia-inducible factor-2alpha mediates the adaptive increase of intestinal ferroportin during iron deficiency in mice, Gastroenterology 140 (2011) 2044–2055.
[16] M.B. Troadec, D.M. Ward, E. Lo, J. Kaplan, I. De Domenico, Induction of FPN1 transcription by MTF-1 reveals a role for ferroportin in transition metal efflux, Blood 116 (2010) 4657–4664.
[17] T. Jiang, B. Harder, M. Rojo de la Vega, P.K. Wong, E. Chapman, D.D. Zhang, p62 links autophagy and Nrf2 signaling, Free Radical Biol. Med. 88 (2015) 199–204.
[18] Y. Chu, Y. Kang, C. Yan, C. Yang, T. Zhang, H. Huo, Y. Liu, LUBAC and OTULIN regulate autophagy initiation and maturation by mediating the linear ubiquitination and the stabilization of ATG13, Autophagy 17 (2021) 1684–1699.
[19] V. Ammanathan, P. Mishra, A.K. Chavalmane, S. Muthusamy, V. Jadhav, C. Siddamadappa, R. Manjithaya, Restriction of intracellular Salmonella replication by restoring TFEB-mediated xenophagy, Autophagy 16 (2020) 1584–1597.

[20] Z. Zhong, A. Umemura, E. Sanchez-Lopez, S. Liang, S. Shalapour, J. Wong, F. He, D. Boassa, G. Perkins, S.R. Ali, M.D. McGeough, M.H. Ellisman, E. Seki, A. B. Gustafsson, H.M. Hoffman, M.T. Diaz-Meco, J. Moscat, M. Karin, NF-kappaB restricts inflammasome activation via elimination of damaged mitochondria, Cell 164 (2016) 896–910.
[21] Y. Ichimura, S. Waguri, Y.S. Sou, S. Kageyama, J. Hasegawa, R. Ishimura, T. Saito, Y. Yang, T. Kouno, T. Fukutomi, T. Hoshii, A. Hirao, K. Takagi, T. Mizushima, H. Motohashi, M.S. Lee, T. Yoshimori, K. Tanaka, M. Yamamoto, M. Komatsu, Phosphorylation of p62 activates the Keap1-Nrf2 pathway during selective autophagy, Mol. Cell 51 (2013) 618–631.
[22] T. Saito, Y. Ichimura, K. Taguchi, T. Suzuki, T. Mizushima, K. Takagi, Y. Hirose, M. Nagahashi, T. Iso, T. Fukutomi, M. Ohishi, K. Endo, T. Uemura, Y. Nishito, S. Okuda, M. Obata, T. Kouno, R. Imamura, Y. Tada, R. Obata, D. Yasuda, K. Takahashi, T. Fujimura, J. Pi, M.S. Lee, T. Ueno, T. Ohe, T. Mashino, T. Wakai, H. Kojima, T. Okabe, T. Nagano, H. Motohashi, S. Waguri, T. Soga, M. Yamamoto, K. Tanaka, M. Komatsu, p62/Sqstm1 promotes malignancy of HCV-positive hepatocellular carcinoma through Nrf2-dependent metabolic reprogramming, Nat. Commun. 7 (2016) 12030.
[23] T. Patinen, S. Adinolfi, C.C. Cortes, J. Harkonen, A. Jawahar Deen, A.L. Levonen, Regulation of stress signaling pathways by protein lipoxidation, Redox Biol. 23 (2019) 101114.
[24] L. Guan, L. Zhang, Z. Gong, X. Hou, Y. Xu, X. Feng, H. Wang, H. You, FoxO3 inactivation promotes human cholangiocarcinoma tumorigenesis and chemoresistance through Keap1-Nrf2 signaling, Hepatology 63 (2016) 1914–1927.
[25] B.D. Manning, A. Toker, AKT/PKB signaling: navigating the network, Cell 169 (2017) 381–405.
[26] K. Inoki, Y. Li, T. Zhu, J. Wu, K.L. Guan, TSC2 is phosphorylated and inhibited by Akt and suppresses mTOR signalling, Nat. Cell Biol. 4 (2002) 648–657.
[27] M. Nairz, D. Ferring-Appel, D. Casarrubea, T. Sonnweber, L. Viatte, A. Schroll, D. Haschka, F.C. Fang, M.W. Hentze, G. Weiss, B. Galy, Iron regulatory proteins mediate host resistance to Salmonella infection, Cell Host Microbe 18 (2015) 254–261.
[28] M. Wlodarska, C.A. Thaiss, R. Nowarski, J. Henao-Mejia, J.P. Zhang, E.M. Brown, G. Frankel, M. Levy, M.N. Katz, W.M. Philbrick, E. Elinav, B.B. Finlay, R.A. Flavell, NLRP6 inflammasome orchestrates the colonic host-microbial interface by regulating goblet cell mucus secretion, Cell 156 (2014) 1045–1059.
[29] L. Ghimire, S. Paudel, L. Jin, P. Baral, S. Cai, S. Jeyaseelan, NLRP6 negatively regulates pulmonary host defense in Gram-positive bacterial infection through modulating neutrophil recruitment and function, PLoS Pathog. 14 (2018), e1007308.
[30] H. Hara, S.S. Seregin, D. Yang, K. Fukase, M. Chamaillard, E.S. Alnemri, N. Inohara, G.Y. Chen, G. Nunez, The NLRP6 inflammasome recognizes lipoteichoic acid and regulates Gram-positive pathogen infection, Cell 175 (2018) 1651–1664, e1614.
[31] P.K. Anand, R.K. Malireddi, J.R. Lukens, P. Vogel, J. Bertin, M. Lamkanfi, T. D. Kanneganti, NLRP6 negatively regulates innate immunity and host defence against bacterial pathogens, Nature 488 (2012) 389–393.
[32] P. Mastroeni, A. Grant, O. Restif, D. Maskell, A dynamic view of the spread and intracellular distribution of Salmonella enterica, Nat. Rev. Microbiol. 7 (2009) 73–80.
[33] S.X. Deng, A.C. Cheng, M.S. Wang, P. Cao, Gastrointestinal tract distribution of Salmonella enteritidis in orally infected mice with a species-specific fluorescent quantitative polymerase chain reaction, World J. Gastroenterol. 13 (2007) 6568–6574.
[34] S. Dichtl, E. Demetz, D. Haschka, P. Tymoszuk, V. Petzer, M. Nairz, M. Seifert, A. Hoffmann, N. Brigo, R. Wurzner, I. Theurl, J.E. Karlinsey, F.C. Fang, G. Weiss, Dopamine is a siderophore-like iron chelator that promotes Salmonella enterica serovar typhimurium virulence in mice, mBio 10 (2019).
[35] L. Wang, L. Harrington, E. Trebicka, H.N. Shi, J.C. Kagan, C.C. Hong, H.Y. Lin, J. L. Babitt, B.J. Cherayil, Selective modulation of TLR4-activated inflammatory responses by altered iron homeostasis in mice, J. Clin. Investig. 119 (2009) 3322–3328.
[36] M. Nairz, G. Weiss, Iron in infection and immunity, Mol. Aspect. Med. 75 (2020) 100864.
[37] C.J. Schmidlin, A. Shakya, M. Dodson, E. Chapman, D.D. Zhang, The intricacies of NRF2 regulation in cancer, Semin. Cancer Biol. 76 (2021) 110–119.
[38] K.K. Jena, S.P. Kolapalli, S. Mehto, P. Nath, B. Das, P.K. Sahoo, A. Ahad, G.H. Syed, S.K. Raghav, S. Senapati, S. Chauhan, S. Chauhan, TRIM16 controls assembly and degradation of protein aggregates by modulating the p62-NRF2 axis and autophagy, EMBO J. 37 (2018).
[39] M. Komatsu, H. Kurokawa, S. Waguri, K. Taguchi, A. Kobayashi, Y. Ichimura, Y. S. Sou, I. Ueno, A. Sakamoto, K.I. Tong, M. Kim, Y. Nishito, S. Iemura, T. Natsume, T. Ueno, E. Kominami, H. Motohashi, K. Tanaka, M. Yamamoto, The selective autophagy substrate p62 activates the stress responsive transcription factor Nrf2 through inactivation of Keap1, Nat. Cell Biol. 12 (2010) 213–223.
[40] C. Camaschella, Iron deficiency, Blood 133 (2019) 30–39.
[41] A.T. Nguyen-Lefebvre, A. Ajith, V. Portik-Dobos, D.D. Horuzsko, A.S. Arbab, A. Dzutsev, R. Sadek, G. Trinchieri, A. Horuzsko, The innate immune receptor TREM-1 promotes liver injury and fibrosis, J. Clin. Investig. 128 (2018) 4870–4883.
[42] X. Hou, R. Zhou, H. Wei, R. Sun, Z. Tian, NKG2D-retinoic acid early inducible-1 recognition between natural killer cells and Kupffer cells in a novel murine natural killer cell-dependent fulminant hepatitis, Hepatology 49 (2009) 940–949.
[43] Z. Dong, M. Huang, Z. Liu, P. Xie, Y. Dong, X. Wu, Z. Qu, B. Shen, X. Huang, T. Zhang, J. Li, J. Liu, T. Yanase, C. Zhou, Y. Xu, Focused screening of mitochondrial metabolism reveals a crucial role for a tumor suppressor Hbp1 in ovarian reserve, Cell Death Differ. 23 (2016) 1602–1614.
[44] L. Sun, S. Yang, Q. Deng, K. Dong, Y. Li, S. Wu, R. Huang, Salmonella effector SpvB disrupts intestinal epithelial barrier integrity for bacterial translocation, Front. Cell. Infect. Microbiol. 10 (2020) 606541.
[45] H.K. De Jong, G.C. Koh, M.H. van Lieshout, J.J. Roelofs, J.T. van Dissel, T. van der Poll, W.J. Wiersinga, Limited role for ASC and NLRP3 during in vivo Salmonella Typhimurium infection, BMC Immunol. 15 (2014) 30.
[46] E.A. Miao, I.A. Leaf, P.M. Treuting, D.P. Mao, M. Dors, A. Sarkar, S.E. Warren, M. D. Wewers, A. Aderem, Caspase-1-induced pyroptosis is an innate immune effector mechanism against intracellular bacteria, Nat. Immunol. 11 (2010) 1136–1142.
[47] B.M. Schultz, G.A. Salazar, C.A. Paduro, C. Pardo-Roa, D.P. Pizarro, F.J. Salazar-Echegarai, J. Torres, C.A. Riedel, A.M. Kalergis, M.M. Alvarez-Lobos, S.M. Bueno, Persistent Salmonella enterica serovar typhimurium infection increases the susceptibility of mice to develop intestinal inflammation, Front. Immunol. 9 (2018) 1166.
[48] X. Yang, S.H. Park, H.C. Chang, J.S. Shapiro, A. Vassilopoulos, K.T. Sawicki, C. Chen, M. Shang, P.W. Burridge, C.L. Epting, L.D. Wilsbacher, S. Jenkitkasemwong, M. Knutson, D. Gius, H. Ardehali, Sirtuin 2 regulates cellular iron homeostasis via deacetylation of transcription factor NRF2, J. Clin. Investig. 127 (2017) 1505–1516.
[49] Y. Li, K. Pan, L. Chen, J.L. Ning, X. Li, T. Yang, N. Terrando, J. Gu, G. Tao, Deferoxamine regulates neuroinflammation and iron homeostasis in a mouse model of postoperative cognitive dysfunction, J. Neuroinflammation 13 (2016) 268.
[50] N.J. Hos, R. Ganesan, S. Gutierrez, D. Hos, J. Klimek, Z. Abdullah, M. Kronke, N. Robinson, Type I interferon enhances necroptosis of Salmonella Typhimurium-infected macrophages by impairing antioxidative stress responses, J. Cell Biol. 216 (2017) 4107–4121.